*Physics – Uspekhi* **59** (9) 886 – 909 (2016) 

*CONFERENCES AND SYMPOSIA*

PACS numbers: **42.60.–v**, **42.79.–e**, 85.70.Sq

# Thermooptics of magnetoactive media: Faraday isolators for high average power lasers

E A Khazanov

DOI: 10.3367/UFNe.2016.03.037829

## Contents



Abstract. **The Faraday isolator, one of the key high-power laser elements, provides optical isolation between a master oscillator and a power amplifier or between a laser and its target, for example, a gravitational wave detector interferometer. However, the absorbed radiation inevitably heats the magnetoactive medium and leads to thermally induced polarization and phase distortions in the laser beam. This self-action process limits the use of Faraday isolators in high average power lasers. A unique property of magnetoactive medium thermooptics is that parasitic thermal effects arise on the background of circular birefringence rather than in an isotropic medium. Also, even insignificant polarization distortions of the radiation result in a worse isolation ratio, which is the key characteristic of the Faraday isolator. All possible laser beam distortions are analyzed for their deteriorating effect on the Faraday isolator parameters. The mechanisms responsible for and key physical parameters associated with different kinds of distortions are identified and discussed. Methods for compensating and suppressing parasitic thermal effects are described in detail, the published experimental data are systematized, and avenues for further research are discussed based on the results achieved.**

**E A Khazanov** Institute of Applied Physics, Russian Academy of Sciences, ul. Ul'yanova 46, 603950 Nizhny Novgorod, Russian Federation
E-mail: khazanov@appl.sci-nnov.ru

Received 2 March 2016
*Uspekhi Fizicheskikh Nauk* **186** (9) 975 – 1000 (2016)
DOI: 10.3367/UFNr.2016.03.037829
Translated by E N Ragozin; edited by A M Semikhatov

**Keywords:** thermal effects in lasers, solid-state lasers with high average power, optical isolation, Faraday isolators

## 1. Introduction

Since the invention of the first laser [1] by T Maiman, one of the main development lines in laser physics has been the increase in the average output power with preservation of a high beam quality: a near-diffraction-limited divergence. The reason lies with the extremely broad range of scientific, technological, and special applications of such lasers. For example, we mention only two proposals published back in the early 1960s: those by Basov and Krokhin concerning the use of lasers for controlled thermonuclear fusion [2] and by Gertsenshtein and Pustovoit about the use of lasers for gravitational wave detection [3]. Recently, the latter idea was successfully realized [4].

Even in the 1960s, for a moderate output power by modern standards, endeavors to increase the output laser power ran into the problem of parasitic thermal effects in the active elements of lasers, especially solid-state ones. For lamp pumping, the heat release power may (sometimes significantly) exceed the output laser power. This is responsible for four parasitic effects: an increase in the volume-average temperature, mechanical damage due to thermally induced stress, the emergence of a thermal lens, and birefringence. The last three effects associated with temperature gradients, which give rise to mechanical stress, are most critical. Damage typically occurs for a heat release power that significantly exceeds the power at which strong phase and polarization distortions occur (the thermal lens and thermally induced depolarization). The thermal lens is caused by the tempera-

ture dependence of the length (linear expansion), the temperature dependence of the refractive index (the $dn/dT$ effect), and the dependence of the refractive index on deformations (the photoelastic effect). Depolarization results from the birefringence caused by the photoelastic effect, which gives rise to thermally induced intrinsic polarizations in an initially isotropic medium. Their direction and phase difference (the magnitude of birefringence) depend on transverse coordinates. As a result, the radiation becomes depolarized upon passing through the sample.

By depolarized radiation, we mean radiation with a polarization that is constant in time but varies from point to point in the transverse cross section. Depolarized radiation is described by a complex electric field amplitude, which is a complex vector function of transverse coordinates. The squared modulus of the complex amplitude defines the intensity of both depolarized and polarized radiation. But the depolarized radiation cannot be characterized by a phase (and, accordingly, by a wavefront) because the phase cannot be introduced for a complex vector.

The first research on thermally induced depolarization was undertaken back in the 1960s [5–7]. In the 1970s, intensive investigations of thermal effects in active laser elements led to the advent of a new line of laser physics — solid-state laser thermooptics [8]. Depolarization was amply and rather promptly studied in glass [9–12] and cubic crystals with orientations [111] [13–17] and [001] [18–20]. Proposed at that time were the still most popular schemes for depolarization compensation: two identical active elements and a 90° polarization rotator placed between them [21] and the combination of an active element, a 45° Faraday rotator, and a mirror [22] (the so-called Faraday mirror).

With an increase in the average laser power, the self-induced thermal effects caused by the absorption of laser radiation itself rather than of the pump have become a problem. The absorption coefficient $\alpha$ in so-called transparent dielectrics ranges from $10^{-6}$ cm$^{-1}$ to $10^{-2}$ cm$^{-1}$. The length $L$ of optical elements varies from several millimeters to several centimeters, and therefore the heat release power can range from a negligible fraction to several percent of the laser power. The peak of research in self-induced thermal effects fell in the 1980s–1990s. Polarization distortions [23, 24] and phase distortions [25, 26] were investigated including those related to the beam shape and cooling conditions [27, 28]. A study was made of the effect of absorption on output laser windows [29, 30], mirrors [30–34], electrooptical modulators [35], and switches [36], as well as frequency doublers [37, 38] and other nonlinear optical elements [39–41].

Standing apart from the others are Faraday isolators (FIs) [42], which are among the key elements of high-power lasers: they provide optical decoupling of either separate laser parts (as a rule, of a master oscillator from a power amplifier) or of the laser itself and the object at which the laser beam is directed. The self-induced thermal effects in an FI are the subject of this paper.

Figure 1 shows the scheme of an FI, whose central element — a Faraday element (FE) — is a magnetoactive medium embedded in a magnetic field. The Faraday effect [43] gives rise to circular birefringence in the FE, with the result that the polarization plane of laser radiation rotates through the angle

$$\Phi = V \int_0^L B(z)\,\mathrm{d}z\,, \tag{1}$$

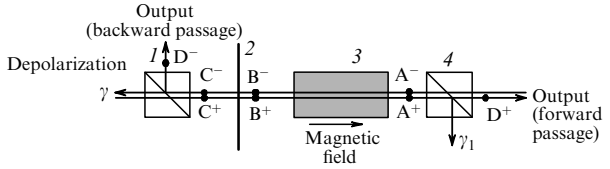


**Figure 1.** Traditional Faraday isolator: *1*, *4* — polarizers, *2* — $\lambda/2$ plate, *3* — FE (45° rotation angle). The letters $A^+-D^+$ and $A^--D^-$ denote planes in the forward and backward passes, respectively. $\gamma_1$ and $\gamma_2$ are nondecouplings (defined in Section 2.2).

where $V$ is the Verdet constant and $L$ is the FE length. Because of the nonreciprocity of the Faraday effect, for $\Phi = 45°$ the beam retains its horizontal polarization (in the plane of the drawing) after a forward passage and passes through polarizer *4*; in the backward passage, the polarization becomes vertical and the beam is, in the ideal case, completely rejected by polarizer *1*. The depolarized radiation passes through polarizer *1*, and its fraction

$$\gamma = \frac{P_{\mathrm{dep}}}{P_0} \tag{2}$$

is called the nondecoupling of the FI. Here, $P_0$ and $P_{\mathrm{dep}}$ are respectively the total radiation power and the power of radiation transmitted through polarizer *1*. *The nondecoupling expressed in decibels,*

$$I = -10 \log \gamma\,, \tag{3}$$

is called the isolation ratio and is the main characteristic of an FI. The level $I = 30-40$ dB is commonly regarded as sufficient. Contributions to the nondecoupling are made by the transverse nonuniformity of the magnetic field, the alignment inaccuracy and contrast of the polarizers, the 'cold' birefringence unrelated to heating, and thermal effects.

The absorption of radiation in the FE gives rise not only to an increase in the volume-averaged temperature but also to a nonuniform temperature distribution over the transverse cross section. This leads to three physical mechanisms acting on laser radiation:

(1) wavefront distortion (a thermal lens) caused by the dependence of the isotropic part of the refractive index on the temperature and mechanical stress, as well as by thermal expansion;

(2) nonuniform distribution of the rotation angle $\Phi$ of the polarization plane caused by the temperature dependence of the Verdet constant, as well as by thermal expansion;

(3) the emergence, along with circular birefringence (the Faraday effect), of linear birefringence arising from mechanical stress due to the presence of a temperature gradient (the photoelastic effect).

The first mechanism induces no polarization changes in laser radiation and therefore has no effect on the nondecoupling and the isolation ratio. The last two mechanisms, by contrast, decrease the isolation ratio. The temperature dependence of the Verdet constant and the thermal expansion lead to a phase difference between eigenpolarizations, which remain circular in this case. The photoelastic effect entails a change not only in the phase difference between the eigenpolarizations but also in the eigenpolarizations themselves, which become elliptical in this case.

From the standpoint of radiation depolarization, Faraday isolators differ in several significant ways from all the previously mentioned optical elements. First, the thermally induced birefringence appears on the background of circular birefringence. Second, the requirements imposed on depolarization in an FI are much more stringent: for instance, a depolarization $\gamma = 1\%$, which is quite admissible in the majority of other elements, leads to a 20 dB isolation ratio in an FI, which is unsatisfactory in general. Third, the thermally induced birefringence in an FE results in an insignificant distortion of the (initially circular) eigenpolarizations, i.e., the eigenpolarizations remain close at all points of the cross section. However, the specific character of the Faraday effect does not allow using circular polarization (close to an eigenpolarization) because the effect of optical decoupling vanishes in this case. Fourth, the relatively high absorption in magnetoactive media, $\alpha \approx (1-3) \times 10^{-3}\ \mathrm{cm}^{-1}$, and the large length of the FE, $L \approx 1-3$ cm, result in a high power of heat release, not less than 0.1% of the laser radiation power.

A thermal lens in an FI was first observed in pulse-periodic lasers with a high repetition rate [44, 45]. The first FI depolarization research [46] was initiated by the Laser Interferometer Gravitational-Wave Observatory (LIGO) project in 1998, which was due not only to the high radiation power but also to the strict requirements imposed on all FI characteristics. The first several years [47–57] saw the first systematic investigations of the thermal effects themselves and of the methods for their compensation and suppression. These results formed the basis for the thermooptics of magnetoactive media, which advanced rapidly in the 2000s and is advancing at the present time. The main results of these investigations are outlined in this paper.

Using the tool of Jones matrices, expressions for the polarization, amplitude, and phase distortions acquired by a laser beam on passing through an FI in forward and backward directions are obtained in Section 2. Parameters responsible for the corresponding distortions are determined. The effects of longitudinal nonuniformity of the magnetic field and the orientation of crystallographic FE axes on the beam shape distortion are considered, as are the special features of using an FE made of ceramics.

Sections 3 and 4 are devoted to the methods for compensating and suppressing thermal effects in FIs. The term compensation is used in reference to the use of FIs with more complex optical setups than that in Fig. 1. They use two optical elements in which the beam distortions are mutually compensated: accumulated in one element and eliminated in the other. We consider setups with the division of one FE into two, as well as setups with a single FE and an additional absorber. Analytic expressions for the nondecoupling and all distortions for all compensation versions are given in tabular form. The methods of depolarization compensation in an FI permitted a significant increase in the power at which the FI provides efficient isolation. The data about FIs are also given in tabular form.

By suppression of distortions we mean their lowering with retention of the FI scheme depicted in Fig. 1. The most radical technique is the cooling of an FI to the boiling temperature of liquid nitrogen, which results in several-fold improvements in many key characteristics of terbium gallium garnet (TGG) crystals — until recently, the only crystal used in FIs for lasers with a high average power at the wavelength $\lambda = 1$ μm. In recent years, many real alternatives to the TGG crystal have appeared; the data about them are given in Section 4.2. We discuss the figures of merit of magnetoactive media in use and the directions of the search for new media. Not the least of the methods for suppressing thermal effects are the enhancement of the magnetic field and the use of the non-rod-shaped geometry of heat removal from an FE. The methods for compensating and suppressing thermal effects in FIs may be used in different combinations with each other.

## 2. Self-induced thermal distortions in radiation propagation through a magnetoactive medium

To investigate thermally induced distortions in an FI, the formalism of Jones matrices [58] can be conveniently used. In Sections 2.1 and 2.2, expressions for the Jones matrix of an FE are obtained, and the polarization and amplitude-phase distortions for the FI depicted in Fig. 1 are determined. We discuss the dependence of these distortions on the parameters of laser radiation and the magnetoactive medium.

### 2.1 Jones matrix of a Faraday rotator with the inclusion of thermal effects

A nonuniformly heated FE is a phase plate in which two kinds of birefringence occur simultaneously: circular due to the Faraday effect and linear due to the photoelastic effect. Circular birefringence is fully described by the phase difference $\delta_c$ (the rotation angle $\Phi$ of the polarization plane being $\delta_c/2$) between the circular eigenpolarizations, and the linear birefringence, by the phase difference $\delta_l$ between the linear eigenpolarizations and the eigenpolarization tilt angle $\Psi$ with respect to the $x$ axis (Fig. 2). This phase plate is described by the Jones matrix [59]

$$F(\delta_c, \delta_l, \Psi) = \exp(\mathrm{i}kLn) \exp\left[\mathrm{i}kLP\big(T(r) - T(0)\big)\right] \times \begin{pmatrix} \cos\dfrac{\delta}{2} - \mathrm{i}\,\dfrac{\delta_l}{\delta}\sin\dfrac{\delta}{2}\cos(2\Psi) & -\dfrac{\delta_c}{\delta}\sin\dfrac{\delta}{2} - \mathrm{i}\,\dfrac{\delta_l}{\delta}\sin\dfrac{\delta}{2}\sin(2\Psi) \\ \dfrac{\delta_c}{\delta}\sin\dfrac{\delta}{2} - \mathrm{i}\,\dfrac{\delta_l}{\delta}\sin\dfrac{\delta}{2}\sin(2\Psi) & \cos\dfrac{\delta}{2} + \mathrm{i}\,\dfrac{\delta_l}{\delta}\sin\dfrac{\delta}{2}\cos(2\Psi) \end{pmatrix}, \tag{4}$$

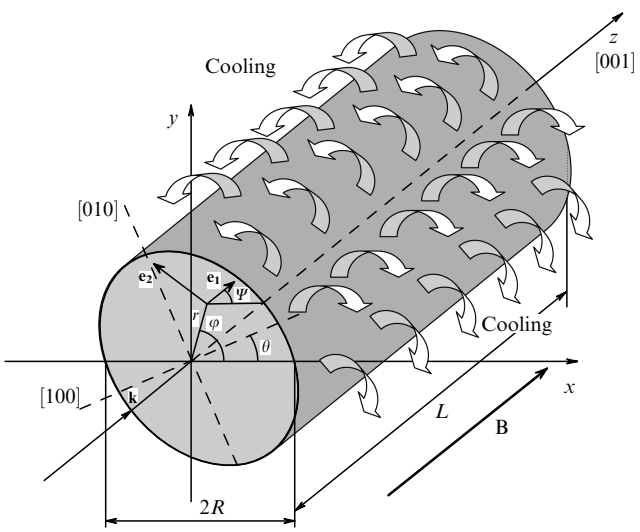


**Figure 2.** Cylindrical FE. $\theta$ is the tilt angle of the crystallographic axis, $\Psi$ is the eigenpolarization tilt angle for a purely linear birefringence, $\mathbf{e}_1$ and $\mathbf{e}_2$ are eigenpolarizations at a point $(r, \varphi)$.

where $n$ is the refractive index,

$$P = \frac{\mathrm{d}n}{\mathrm{d}T} - \frac{1}{L}\frac{\mathrm{d}L}{\mathrm{d}T}\frac{n_0^3}{4}\frac{1+\nu}{1-\nu}(p_{11}+p_{12}) \tag{5}$$

is the thermooptical constant, $k = 2\pi/\lambda$, $\delta^2 = \delta_l^2 + \delta_c^2$, $n_0$ is the 'cold' refractive index, $\nu$ is the Poisson coefficient, and $p_{ij}$ are elements of the elasto-optical tensor (photoelastic coefficients). Here and hereafter, we assume that the FE is a cubic crystal of m3m symmetry in the shape of a long cylinder of the [001] orientation and that the diffraction beam length greatly exceeds the FI length even with the inclusion of the induced distortions. The exponential factor in expression (4) (which is borrowed from Ref. [8]) does not affect the polarization distortions and describes an isotropic thermal lens. The contribution to this lens is made by the temperature dependence of the refractive index and the 'isotropic' part of the photoelastic effect [two terms in expression (5)]. The contribution of thermal expansion to the thermal lens is typically negligible in comparison with the contribution of the temperature dependence of the refractive index, and the corresponding term is therefore omitted from expression (5).

The values of $\delta_l$ and $\Psi$ are expressed in [8, 20] in terms of the temperature distribution $T(r)$ and the angle $\theta$ (see Fig. 2) between the crystallographic axis and the $x$ axis:

$$\delta_l = 2kLQ\sqrt{\cos^2(2\varphi - 2\theta) + \xi^2\sin^2(2\varphi - 2\theta)} \times \left(\frac{1}{r^2}\int_0^r r^2\frac{\mathrm{d}T}{\mathrm{d}r}\,\mathrm{d}r\right), \tag{6}$$

$$\tan(2\Psi - 2\theta) = \xi\tan(2\varphi - 2\theta), \tag{7}$$

where

$$Q = \frac{1}{L}\frac{\mathrm{d}L}{\mathrm{d}T}\frac{n_0^3}{4}\frac{E_s}{1-\nu}(\pi_{11}-\pi_{12}) = \frac{1}{L}\frac{\mathrm{d}L}{\mathrm{d}T}\frac{n_0^3}{4}\frac{1+\nu}{1-\nu}(p_{11}-p_{12}), \tag{8}$$

$$\xi = \frac{\pi_{44}}{\pi_{11}-\pi_{12}} = \frac{2p_{44}}{p_{11}-p_{12}}, \tag{9}$$

$E_s$ is the Young modulus, and $\pi_{ij}$ are elements of the elastooptic tensor. The quantity $\xi$ is called the optical anisotropy parameter [8] and $Q$ is the thermooptical constant [8]. The two expressions for $\xi$ and $Q$ are equivalent, strictly speaking, only when the anisotropy of the elastic compliance tensor may be neglected. In general, the expression in terms of the $\pi$ tensor must be used [60].

Let an FE with an absorption coefficient $\alpha \ll 1/L$ and a heat conductivity coefficient $\kappa$ be heated by a Gaussian beam of radius $r_0$ at an intensity level of 1/e and power $P_0$. Then, setting $\mathrm{d}T/\mathrm{d}z = 0$ in the heat conduction equation, we find the temperature gradient

$$\frac{\mathrm{d}T}{\mathrm{d}r} = -\frac{\alpha P_0}{2\pi\kappa}\frac{1-\exp(-r^2/r_0^2)}{r}. \tag{10}$$

Substituting Eqn (10) in expression (6) and integrating, we obtain

$$\delta_l(r,\varphi) = p\,\frac{r^2/r_0^2 + \exp(-r^2/r_0^2) - 1}{r^2/r_0^2} \times \sqrt{\cos^2(2\varphi - 2\theta) + \xi^2\sin^2(2\varphi - 2\theta)}, \tag{11}$$

where

$$p = \frac{L}{\lambda}\frac{\alpha Q}{\kappa}P_0. \tag{12}$$

The value of $\delta_c$ is determined by the Faraday effect with the temperature dependence of the Verdet constant $V$ taken into account:

$$\delta_c(r) = \delta_{c0}\left[1 + \frac{1}{V}\frac{\mathrm{d}V}{\mathrm{d}T}\big(T(r) - T(r^*)\big)\right], \tag{13}$$

where $\delta_{c0} = 2VBL = 2\Phi$ is the double angle of polarization rotation for $r = r^*$; the value of $r^*$ can be chosen so as to minimize depolarization (see Section 2.2). Typically, $|(1/V)(\mathrm{d}V/\mathrm{d}T)|$ is much greater than the linear expansion coefficient, and we therefore ignored the contribution of the latter to expression (13).

Thus, with expressions (5), (7), (11), and (13), expression (4) completely determines the Jones matrix of an FE.

### 2.2 Polarization distortion (depolarization) of radiation

We find the nondecoupling of an FI and determine which physical effect makes the greatest contribution to it. In the absence of a thermal effect in an FE, after two passes, the beam changes polarization to the vertical one (perpendicular to the plane of Fig. 1) and is reflected by polarizer *1*. Owing to thermal effects, depolarized radiation appears, which has horizontal polarization at a point $C^-$ and passes through polarizer *1*. The intensity fraction of this radiation defines the local nondecoupling $\Gamma(r,\varphi)$:

$$\Gamma(r,\varphi) = \frac{|\mathbf{E}_C\mathbf{x}_0|^2}{|\mathbf{E}_C|^2}, \tag{14}$$

where $\mathbf{E}_C$ is the complex field amplitude at the point $C^-$ and $\mathbf{x}_0$ is a unit vector. The cross-section-integrated nondecoupling $\gamma$ in (2) — the depolarized radiation power fraction — is given by

$$\gamma = \frac{1}{\pi r_0^2}\int_0^{2\pi}\mathrm{d}\varphi\int_0^\infty \Gamma\exp\left(-\frac{r^2}{r_0^2}\right)r\,\mathrm{d}r, \tag{15}$$

where we assume that the optical diameter of the FE is such that the aperture loss may be disregarded and the integration over $r$ in (15) can be extended to infinity.

Let the beam have a Gaussian shape and be horizontally polarized at a point $A^-$ in the backward passage through the FI:

$$\mathbf{E}(A^-) = \text{const}\,\mathbf{x}_0\exp\left(-\frac{r^2}{2r_0^2}\right). \tag{16}$$

When the Jones matrices are known for all optical elements, the field at the point $C^-$ is easily found:

$$\mathbf{E}(C^-) = L_2\left(\frac{3\pi}{8}\right)F\left(\delta_{c0} = \frac{\pi}{2}, \delta_l\right)\mathbf{E}(A^-), \tag{17}$$

where $L_2(\beta_L)$ is the matrix of the $\lambda/2$ plate with an optical axis tilt angle $\beta_L$:

$$L_2(\beta_L) = \begin{pmatrix} \cos(2\beta_L) & \sin(2\beta_L) \\ \sin(2\beta_L) & -\cos(2\beta_L) \end{pmatrix}. \tag{18}$$

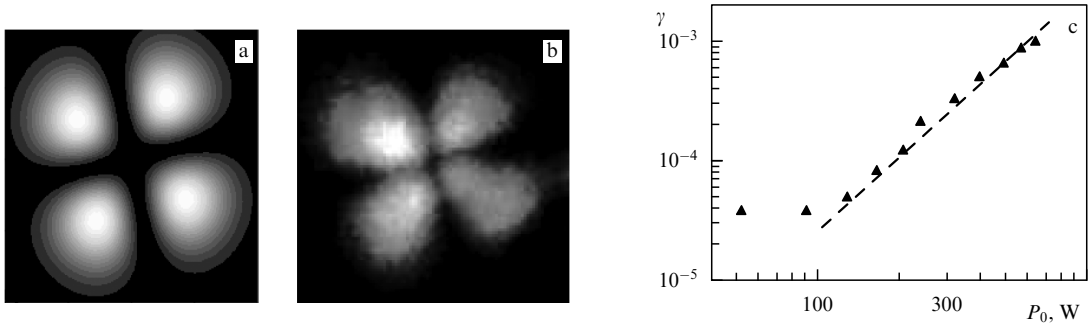


**Figure 3.** (a) Theoretical and (b) experimental [49] spatial depolarization distribution $\Gamma(r,\varphi)$. (c) Dependence of $\gamma$ on the radiation power $P_0$ (from Ref. [67]).

Substituting expressions (4), (16), and (18) in (17) and then substituting the result in (14) and (15), we can find local ($\Gamma$) and integral ($\gamma$) depolarizations. We consider the case where the linear birefringence is small,

$$\delta_{\rm l} \ll 1\,. \tag{19}$$

We also assume that the temperature-induced variations of the rotation angle of the polarization plane are much smaller than the angle itself: $\delta_{\rm c}(r) - \delta_{\rm c0} \ll \delta_{\rm c0}$. From (14), in view of inequality (19), up to the terms of the order of $\delta_{\rm l}^4$ and $\delta_{\rm l}^2(\delta_{\rm c} - \delta_{\rm c0})$, we then obtain

$$\Gamma(r,\varphi) = \Gamma_p(r,\varphi) + \Gamma_V(r) = \frac{2\delta_{\rm l}^2}{\pi^2}\sin^2\left(2\Psi(r,\varphi) - \frac{\pi}{4}\right) + \left(\frac{\delta_{\rm c}(r)}{2} - \frac{\pi}{4}\right)^2. \tag{20}$$

We substitute expressions (7), (11), and (13) in formula (20) and then substitute the result in expression (15) to obtain

$$\gamma = A_p p^2\left[1 + (\xi^2 - 1)\cos^2\left(\frac{\pi}{4} - 2\theta\right)\right] + \frac{\pi^2}{8r_0^2}\left(\frac{1}{V}\frac{{\rm d}V}{{\rm d}T}\right)^2 \int_0^\infty \exp\left(-\frac{r^2}{r_0^2}\right)\left(T(r) - T(r^*)\right)^2 r\,{\rm d}r\,. \tag{21}$$

In the subsequent discussion, $A_p$ (as well as $A$ with other subscripts) are constants whose values are collected in Table 2 in Section 3.3. By rotating the FE about the $z$ axis, i.e., by selecting the optimal angle $\theta = \theta_{\rm opt}$, it is possible to minimize the first term in expression (21). It is easily seen that $\theta_{\rm opt} = 3\pi/8$ when $|\xi| > 1$ and $\theta_{\rm opt} = \pi/8$ when $|\xi| < 1$. Similarly, by equating the derivative of (21) with respect to $r^*$ to zero, we find the optimal value $r_{\rm opt} \approx 0.92 r_0$. In practice, the magnetic field should be chosen such that the rotation angle of the polarization plane be $\Phi = \pi/4$ at the point $r = 0.92 r_0$ [see formula (13)]. As a result of these two optimizations, we obtain

$$\gamma = \gamma_p + \gamma_V\,, \tag{22}$$

where

$$\gamma_p = \begin{cases} A_p p^2\,, & |\xi| \geqslant 1\,, \\ A_p p^2 \xi^2\,, & |\xi| < 1\,, \end{cases} \tag{23}$$

$$\gamma_V = A_V p_V^2\,, \tag{24}$$

$$p_V = \frac{\alpha P_0}{8\kappa}\,\frac{1}{V}\frac{{\rm d}V}{{\rm d}T}\,. \tag{25}$$

We note that both $\gamma_p$ and $\gamma_V$ are independent of the beam radius $r_0$ and are proportional to the square of the radiation power $P_0$. Therefore, nondecoupling (20)–(22) is the sum of two terms corresponding to two physical mechanisms: the photoelastic effect and the temperature dependence of the Verdet constant. By equating expressions (23) and (24), we obtain the FE length $L^*$ at which $\gamma_V = \gamma_p$, i.e., the contributions to depolarization from the photoelastic effect and the temperature dependence of $V$ are equal:

$$L^* = \begin{cases} \sqrt{\dfrac{A_V}{A_p}}\,\dfrac{\lambda}{8Q}\left(\dfrac{1}{V}\dfrac{{\rm d}V}{{\rm d}T}\right), & |\xi| \geqslant 1\,, \\ \sqrt{\dfrac{A_V}{A_p}}\,\dfrac{\lambda}{8Q\xi}\left(\dfrac{1}{V}\dfrac{{\rm d}V}{{\rm d}T}\right), & |\xi| < 1\,. \end{cases} \tag{26}$$

In most cases, $L \gg L^*$ and $\gamma_V \ll \gamma_p$, i.e., the photoelastic effect prevails, which was first shown in Ref. [48]. The transverse nondecoupling distribution $\Gamma(r,\varphi)$ is the most obvious experimental proof of this circumstance. According to formula (20), the distribution $\Gamma_V$ is independent of $\varphi$, while $\Gamma_p$ has the shape of a cross, the axes of this cross being turned through the angle $\Phi/2 = \pi/8$ relative to the $x$ and $y$ axes, which was first demonstrated in Ref. [49] (Fig. 3a). Furthermore, numerous experiments in depolarization compensation (see Section 3.2) also confirm that the temperature dependence of the Verdet constant may be ignored. Exceptions are provided by cryogenic FIs, which are discussed in Section 4.1, and the terbium–scandium–aluminum garnet (TSAG) (see Section 4.2).

To compare different FIs, in practice, it is convenient to introduce the maximal admissible radiation power $P_{\rm max}$, on reaching which $\gamma$ and $I$ take the maximal admissible values defined by specific applications; for definiteness, we assume the respective values 0.001 and 30 dB.

The thermal effects in the FI depicted in Fig. 1, which is hereinafter referred to as a traditional FI, were experimentally studied in many papers [49, 52, 61–73] for the laser radiation power up to 800 W. The main results of these investigations are given in the upper part of Table 3.

For example, Fig. 3c shows the experimental data in Ref. [67]. For a low power, the nondecoupling $\gamma$ is independent of $P_0$ and is determined by the 'cold' FE depolarization, the contrast ratio of the polarizers, and the nonuniformity of the magnetic field. The nondecoupling $\gamma$ increases with power and tends to the theoretical dependence $\gamma_p$ in (23) for a high power. As is clear from Table 3, $P_{\rm max}$ is currently not more than 650 W for traditional TGG crystal FIs, while the TSAG

crystal (see Section 4.2) recently permitted reaching $P_{\max} \approx 1.5$ kW [74].

Polarization distortions in FIs are important not only in the backward radiation passage but also in the forward one (from left to right in Fig. 1), because they result in power loss. We let $\gamma_1$ denote the fraction of radiation power with the vertical polarization at the point $A^+$. For $\theta = \theta_{\text{opt}}$, the expression for $\gamma_1$ including only the photoelastic effect is [51]

$$\gamma_1 = \begin{cases} A_p \xi^2 , & |\xi| \geqslant 1 , \\ A_p p^2 , & |\xi| < 1 . \end{cases} \tag{27}$$

### 2.3 Properties of radiation depolarization in Faraday mirrors

Before discussing amplitude–phase distortions in FIs, we briefly consider the features of depolarization in a Faraday mirror, whose operation is shown schematically in Fig. 4. Unlike an FI, a Faraday mirror has no polarizers and is used not for optical decoupling but, as a rule, for compensating the birefringence in the active elements of high-power laser systems. After two passes through the FE, the polarization rotates through 90°, with the result that the linear polarization is recovered. This idea, which was first proposed in Ref. [22] and then 'rediscovered' over and over again [75–77], is used in solid-state laser amplifiers [78–81], oscillators [82–84], and regenerative amplifiers [85], as well as in fiber optics [86, 87] and semiconductor lasers [88].

Evidently, if the Faraday mirror itself introduces polarization distortions (depolarization), the compensation of the birefringence in an active element must be incomplete. Despite the considerable similarity between the FI and the Faraday mirror, there are two important differences between them, which are of fundamental importance in the investigation of thermal effects.

First, the nondecoupling of an FI is affected only by the depolarization in the second passage, while the polarization distortions in a Faraday mirror are accumulated during both passages. Apart from an obvious quantitative consequence, this has a more important qualitative consequence. Owing to the nonreciprocity of the Faraday effect, new FIs (see Section 3) efficiently compensate depolarization in the backward passage but hardly decrease it in the forward one.

Second, the radiation incident on an FI is always linearly polarized in a certain direction; therefore, for an efficient decoupling it would suffice that only this linear polarization be slightly distorted in the backward passage. By contrast, the radiation already depolarized in the active element is incident on the Faraday mirror. It is therefore required that the

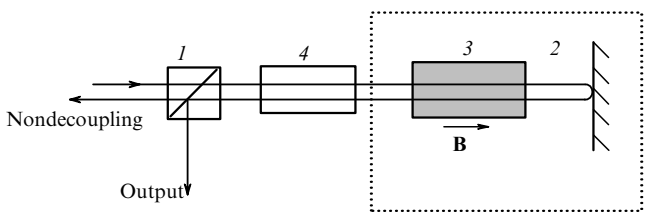


**Figure 4.** Schematic for depolarization compensation in active elements with the use of a Faraday mirror (dotted rectangle): *1* — polarizer, *2* — mirror, *3* — Faraday element with a 45° rotation angle, *4* — active element.

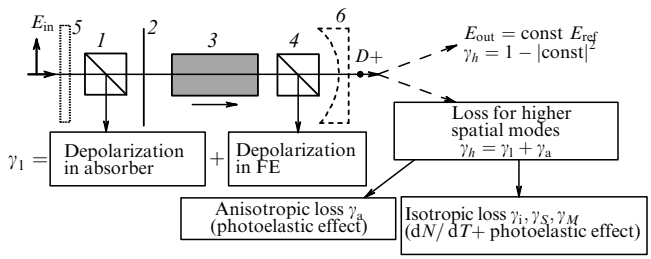


**Figure 5.** Laser radiation distortions in the direct passage through an FI: *1*, *4* — polarizers, *2* — $\lambda/2$ plate, *3* — FE (45° rotation angle), *5* — absorbing optical element with a negative thermal lens, *6* — compensating negative lens or telescope.

Faraday mirror rotate any polarization through 90° without distorting it.

A detailed discussion of the operation of a high-power Faraday mirror is beyond the scope of this paper. We only mention Refs [53, 56, 89] concerned with theoretical and experimental investigations of Faraday mirrors, including a method for improving their operation for a high average radiation power.

### 2.4 Amplitude–phase distortions in Faraday isolators

Apart from polarization distortions, spatial (amplitude and phase) thermal distortions emerge in the output radiation $\mathbf{E}_{\text{out}}$. The output beam may be the beam at points $D^-$ and /or $D^+$, depending on the specific version of the FI (see Fig. 1). Here, we restrict ourselves to the more frequent second case. To describe the spatial distortions of the output radiation quantitatively, we use the quantity $\gamma_h$ — the deviation from unity of the overlap integral $H$ of the laser field $E_{\text{out}}$ and the ideal field $E_{\text{ref}}$ that would occur in the absence of thermal effects ($\delta_l = 0$) (Fig. 5):

$$\gamma_h = 1 - H = 1 - \frac{\left| \int_0^{2\pi} \mathrm{d}\varphi \int_0^{\infty} E_{\text{out}} E_{\text{ref}}^* r \, \mathrm{d}r \right|^2}{\int_0^{2\pi} \mathrm{d}\varphi \int_0^{\infty} |E_{\text{out}}|^2 r \, \mathrm{d}r \int_0^{2\pi} \mathrm{d}\varphi \int_0^{\infty} |E_{\text{ref}}|^2 r \, \mathrm{d}r} . \tag{28}$$

We emphasize that $\gamma_h$ may be a no less important characteristic of the FI than the isolation ratio. As an example, we mention the laser interferometer for detecting gravitational waves [32].

In Ref. [51], with the Jones matrix used to find the field $\mathbf{E}_{\text{out}}$ for weak polarization distortions (19) and weak phase distortions, $kL(n(r) - n(0)) \ll 1$, an analytic expression was derived for $\gamma_h$ at $\theta = \theta_{\text{opt}}$:

$$\gamma_h = \gamma_{\text{i}} + \gamma_{\text{a}} , \tag{29}$$

where

$$\gamma_{\text{a}} = \begin{cases} A_p p^2 , & |\xi| \geqslant 1 , \\ A_p p^2 \xi^2 , & |\xi| < 1 , \end{cases} \tag{30}$$

$$\gamma_{\text{i}} = A_{\text{i}} p_{\text{i}}^2 , \tag{31}$$

$$p_{\text{i}} = \frac{L}{\lambda} \frac{\alpha P}{\kappa} P_0 . \tag{32}$$

We note that the isotropic ($\gamma_{\text{i}}$) and anisotropic ($\gamma_{\text{a}}$) losses (like $\gamma_p$, $\gamma_V$, and $\gamma_1$) are independent of the beam radius $r_0$ and are proportional to the squared heating radiation power $P_0$. Two physical effects contribute to $\gamma_h$ in (29): an isotropic

thermal lens, which, we note, is not parabolic, and radiation depolarization. The contribution of the second effect is caused by the fact that the depolarization is not uniform over the cross section, and the beam therefore acquires amplitude and phase distortions on passing through polarizer *4*. Hence, on passing through the FI, the total thermally induced power loss of a spatial polarization mode is $\gamma_{\text{total}} = \gamma_1 + \gamma_{\text{a}} + \gamma_{\text{i}}$.

Isotropic power loss is conveniently characterized by not only a decrease in the overlap integral $H$ in (28) but also a decrease in the Strehl number $S$ [90, 91] and/or an increase in the beam quality parameter $M^2$ [92]:

$$\gamma_S = 1 - S\,, \qquad \gamma_M = 1 - \left(\frac{M_{\text{in}}^2}{M_{\text{out}}^2}\right)^2 . \tag{33}$$

A detailed analysis was performed in Ref. [93], with the following expression derived in the case of small distortions:

$$\gamma_S = A_S\, p_{\text{i}}^2\,, \qquad \gamma_M = A_M\, p_{\text{i}}^2\,. \tag{34}$$

Therefore, isotropic losses (31) and (34) are proportional, up to numerical factors $A_{\text{i}}$, $A_S$, and $A_M$ tabulated in Table 2 below, to the square of $p_{\text{i}}$. The $p_{\text{i}}$ parameter in (32) is similar to $p$ in (12), up to the replacement of the thermooptical constant $Q$ (8), which characterizes anisotropic distortions, with the thermooptical constant $P$ (5), which characterizes isotropic distortions. Isotropic distortions $\gamma_{\text{i}}$, $\gamma_S$, and $\gamma_M$ are determined only by the $p_{\text{i}}$ parameter, while $p$ determines the photoelasic-effect-induced polarization $\gamma_1$ and amplitude $\gamma_{\text{a}}$ losses, as well as the nondecoupling $\gamma_p$. We note that the photoelasic effect also makes a contribution to the isotropic loss $\gamma_{\text{i}}$ [see the second term in expression (5)]. Expressions (29)–(31), (34) were derived for weak distortions. In general, the data of numerical integration suggest that these expressions are highly accurate as long as the values of $\gamma_{\text{a}}$, $\gamma_{\text{i}}$, $\gamma_S$, and $\gamma_M$ are less than 0.1.

Because the thermal phase depends on $r$ nonparabolically, the distortion is conveniently represented in the form of an ideal thermal lens with a focal distance $F$ and a phase aberrator with a zero geometrical divergence. Using the method of moments [94], the following expression can be obtained for $F$ [95]:

$$F = A_F\, \frac{k r_0^2}{p_{\text{i}}}\,. \tag{35}$$

For a Gaussian beam, $A_F = 2$. In several papers, formula (35) is quoted with $A_F = 1$, which is true for a rectangular beam (see Section 2.6) but incorrect for a Gaussian one.

We note that maximizing the Strehl number requires using a compensating lens with a focal length significantly different from that in formula (35) (see Section 3.3). All said above about isotropic distortions applies not only to FIs but also to any other optical elements.

### 2.5 Effect on the distortion of longitudinal nonuniformity of a magnetic field

In the foregoing, we assumed that the magnetic field $B$ is independent of the longitudinal coordinate $z$. In the absence of thermal effects, the $z$-dependence of $B$ is of no importance, because only the integral of $B$ enters (1). But the $B(z)$ dependence 'manifests itself' under a thermal load. Then $\delta_{\text{c}}$, as well as the ellipticity of eigenpolarizations, becomes a function of $z$. The Jones matrices cannot be used in this case. To calculate the evolution of the polarization ellipse in the course of propagation through a medium whose eigenpolarizations depend on $z$, it is convenient to use the tool [96, 97] of a complex variable $\chi$ defined as the ratio of the complex electric field amplitudes in circular polarizations. In Ref. [98], an expression relating the value $\chi(L)$ at the FE output to the value $\chi(0)$ at the FE input was obtained in the form

$$\chi(L) = \exp\left(-\mathrm{i}\delta_{\text{c}}(L)\right)\left[\chi(0) - \frac{\mathrm{i}\delta_1}{2L}\int_0^L \left[\exp\left(2\mathrm{i}\Psi + \mathrm{i}\delta_{\text{c}}(z)\right) - \chi^2(0)\exp\left(-2\mathrm{i}\Psi - \mathrm{i}\delta_{\text{c}}(z)\right)\right]\mathrm{d}z + O(\delta_1^2)\right], \tag{36}$$

together with the expression [48]

$$\Gamma_p = \frac{\delta_1^2}{4}\left[\frac{1}{L}\int_0^L \sin\left(2\Psi - \delta_{\text{c}}(z)\right)\mathrm{d}z\right]^2, \tag{37}$$

which passes into the first term in Eqn (20) in the case of a uniform magnetic field, $\delta_{\text{c}}(z) = z\delta_{\text{c}0}/L$. Taking nonuniformity into account leads to insignificant corrections; but the longitudinal profile of the magnetic field can be of major importance for FIs with depolarization compensation, as discussed in Section 3.1. Furthermore, a strong nonuniformity can be used to decrease the depolarization.

### 2.6 Effect on the beam shape distortion

In Sections 2.1–2.5, we considered self-induced thermal distortions of a Gaussian beam. Because the laser beam simultaneously records distortions (being a source of heat) and reads them, the magnitude of self-action depends on the transverse intensity distribution. The results obtained above were generalized in Ref. [56] to an arbitrary axially symmetric beam. Here, we restrict ourselves to the consideration of a super-Gaussian beam:

$$\mathbf{E}(\mathrm{A}^-) = \text{const}\ \mathbf{x}_0 \exp\left(-\frac{r^{2m}}{2r_0^{2m}}\right). \tag{38}$$

The parameter $m$ characterizes the rate of intensity decrease. For $m = 1$ (a Gaussian beam) the intensity decreases rather slowly. As $m$ increases, the rate of intensity decrease becomes higher, and the beam transforms into a rectangular-shaped beam for $m = \infty$.

When the calculations described in Sections 2.2 and 2.4 are repeated for a laser beam obeying formula (38) [instead of formula (16)], it can be shown that the nondecoupling $\gamma_p$ in (23) and $\gamma_V$ in (24), the forward-passage loss $\gamma_1$ in (27), $\gamma_{\text{a}}$ and $\gamma_{\text{i}}$ in (31), $\gamma_S$ and $\gamma_M$ in (34), as well as the focal length of a thermal lens $F$ in (35), remain valid for any $m$ if all the corresponding constants $A$ are replaced with the quantities $A(m)$ whose expressions are collected in Table 2. Therefore, the beam shape affects only the numerical factor, which decreases with increasing $m$. This signifies that all distortions become weaker in passing from a Gaussian beam to a rectangular-shaped one. Therefore, rectangular-shaped beams are optimal from the standpoint of minimizing the influence of all thermal effects, while Gaussian beams experience the strongest self-action. At the same time, focal length (35) of a thermal lens for a Gaussian beam is two times longer than for a rectangular-shaped one: $A_F = A_F(m = 1) = 2A_F(m = \infty)$.

The ratio $\gamma_V/\gamma_p$ is proportional to $A_V(m)/A_p(m)$ [see formulas (23) and (24)], i.e., it decreases with increasing $m$.

Therefore, the conclusion that the contribution of the temperature dependence of the Verdet constant is negligible, which was reached in Section 2.2 for Gaussian beams, remains valid for any beam of shape (38).

### 2.7 Crystals of other orientations and optical ceramics

The results in Sections 2.1–2.6 apply to a cubic crystal of the [001] orientation and m3m symmetry inherent in TGG crystals employed in the majority of FIs. The use of other crystals, including those with m3 symmetry, is discussed in Section 4.2.

The analysis performed in Ref. [54] for a TGG crystal of an arbitrary orientation showed that the [001] orientation is optimal because it permits obtaining the highest isolation ratio. The [111] orientation is the worst one. Thermooptical distortions are such that all formulas for the [111] orientation can be obtained from the corresponding formulas for [001] by the formal substitution [8, 20, 98]

$$\xi_{111} = 1\,, \quad Q_{111} = Q\,\frac{1+2\xi}{3}\,, \quad P_{111} = P + Q\,\frac{1-\xi}{3}\,. \qquad (39)$$

The use of ceramic FEs instead of single-crystal ones was proposed in Ref. [89]. The features of thermal effects in ceramics were comprehensively studied in several papers [99–101]. In FIs, small-scale thermal effects related to the grain size are weak [102], and it can be assumed in practice that a ceramic element is equivalent to the single-crystal one with the thermooptical constants [103, 104]

$$\xi_{\text{ceramic}} = 1\,, \quad Q_{\text{ceramic}} = Q\,\frac{2+3\xi}{5}\,, \quad P_{\text{ceramic}} = P + Q\,\frac{1-\xi}{5}\,. \qquad (40)$$

The nondecoupling $\gamma_p$ in (23) and the losses $\gamma_1$ in (27) and $\gamma_a$ in (31) are proportional to $Q^2$. Consequently, for a TGG crystal ($\xi = 2.25$), we obtain the ratio $\gamma_{001}{:}\gamma_{111}{:}\gamma_{\text{ceramic}} = 1{:}3.4{:}3.1$. In other words, ceramics are slightly better than the crystal of the [111] orientation, but are 3.1 times worse than a crystal of the [001] orientation. We note that crystals of the [111] orientation enjoy wide use. Furthermore, an important advantage of [111] crystals and ceramics is the simplicity of alignment, because depolarization is independent of the angle $\theta$ [see expression (21) for $\xi = 1$], while a crystal with the [111] orientation requires precise alignment: $\theta = \theta_{\text{opt}}$. We note that $Q_{111}(\xi = -0.5) = 0$ and $Q_{\text{ceramic}}(\xi = -2/3) = 0$, i.e., the depolarization arising from the photoelastic effect vanishes completely.

For TGG, $P/Q = 10$ and therefore $P_{111} \approx P_{\text{ceramic}} \approx P$, and hence $p_{\text{i}}$ and $\gamma_{\text{i}}$ in (31), $\gamma_S$ and $\gamma_M$ in (34), and $F$ in (35) are practically the same in all three cases. The quantity $\gamma_V$ is independent of the crystal orientation. Finally, for all glass materials, $\xi = 1$, while $P$ and $Q$ remain invariable:

$$\xi_{\text{glass}} = 1\,, \quad Q_{\text{glass}} = Q\,, \quad P_{\text{glass}} = P\,. \qquad (41)$$

Therefore, all results, including those outlined below, for crystals of the [001] orientation can be easily generalized to crystals of the [111] orientation, ceramics, and glass using respective formulas (39), (40), and (41).

## 3. Compensation of thermal effects in Faraday isolators

By the compensation of self-induced thermal distortions, we mean the use of FIs with more complex optical configurations than that depicted in Fig. 1. The main idea is to use two optical elements in which the beam distortions cancel each other: they are accumulated in one of them and eliminated in the other. In Sections 3.1 and 3.2, we consider FIs both with division of one FE into two and with a single FE and an additional absorber. Of greatest interest is the compensation of depolarization, because it increases the isolation ratio, which is the main FI parameter. Ways to compensate a thermal lens are discussed in Section 3.3.

### 3.1 Depolarization compensation. Theory

As shown in Section 2, the main cause of depolarization and hence of a decrease in the isolation ratio is the photoelastic effect. It is well known that a 90° polarization rotator located between any two similar phase plates with linear eigenpolarizations gives rise to complete depolarization compensation [21]. When there is also circular birefringence in these plates, the statement is true only when their birefringence has the opposite sign. This is unacceptable in the making of an FI, because the nonreciprocal properties of the isolator then vanish. The author of Ref. [47] proposed the idea of replacing one 45° FE by two 22.5° ones and a $\lambda/2$ plate (Fig. 6a) or a 67.5° reciprocal rotator (RR) with polarization (Fig. 6b) between them. Below, these new isolators are referred to as FIs with a $\lambda/2$ plate and FIs with an RR.

Apart from the efficiency of these FIs (see below), of interest is the possibility of using an optical element located outside a traditional FI, beyond the magnetic field for the purpose of depolarization compensation. The idea is to make a phase plate that would subtract all phase shifts acquired by the beam in an FE. To do this, the phase plate must have the same transverse eigenpolarization distribution as the FE and its transverse phase-difference distribution must be of the same amplitude but of the opposite sign. It was suggested

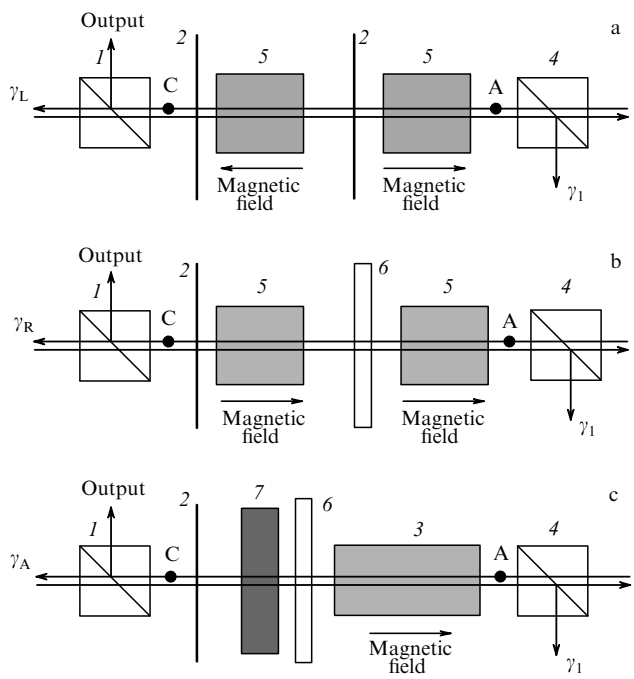


**Figure 6.** FI with depolarization compensation: (a) FI with a $\lambda/2$ plate, (b) FI with a reciprocal rotator, (c) FI with an absorber element. *1*, *4* — polarizers, *2* — $\lambda/2$ plates, *3* — FE (45° rotation angle), *5* — FE (22.5° rotation angle), *6* — reciprocal polarization rotator (67.5° rotation angle), *7* — optical absorber.

in [57] that crystal quartz placed in a diverging beam should be used as such a plate. A polarization decrease by nearly an order of magnitude was experimentally demonstrated. However, this method has not gained wide acceptance because optimal compensation requires alignment when the laser power is changed. The FI proposed in Ref. [65] (Fig. 6c) is free from this drawback; the role of such a plate is played by a 67.5° polarization rotator and an optical radiation absorber element (AE), in which thermally induced birefringence appears. This isolator is referred to as an FI with an AE below.

We find the nondecoupling of the FIs depicted in Fig. 6, as was done in Section 2.2. When the Jones matrices are known for all optical elements, it is easy to find the field **E** at point C (hereinafter, the indices L, R, and A respectively denote the FIs in Fig. 6a, b, and c):

$$\mathbf{E}_{\mathrm{L}}(\mathrm{C}) = L_2\left(\beta_{\mathrm{L}} + \frac{\pi}{8}\right) F\left(\delta_{\mathrm{c}} = -\frac{\pi}{4}, \frac{\delta_{\mathrm{l}}}{2}\right) \times L_2(\beta_{\mathrm{L}})\, F\left(\delta_{\mathrm{c}} = \frac{\pi}{4}, \frac{\delta_{\mathrm{l}}}{2}\right)\mathbf{E}(\mathrm{A}), \tag{42}$$

$$\mathbf{E}_{\mathrm{R}}(\mathrm{C}) = L_2\left(\frac{\beta_{\mathrm{R}}}{2} + \frac{3\pi}{8}\right) F\left(\delta_{\mathrm{c}} = \frac{\pi}{4}, \frac{\delta_{\mathrm{l}}}{2}\right) \times R(\beta_{\mathrm{R}})\, F\left(\delta_{\mathrm{c}} = \frac{\pi}{4}, \frac{\delta_{\mathrm{l}}}{2}\right)\mathbf{E}(\mathrm{A}), \tag{43}$$

$$\mathbf{E}_{\mathrm{A}}(\mathrm{C}) = L_2\left(\frac{\beta_{\mathrm{A}}}{2} + \frac{3\pi}{8}\right) F(\delta_{\mathrm{c}} = 0, D\delta_{\mathrm{l}}) \times R(\beta_{\mathrm{A}})\, F\left(\delta_{\mathrm{c}} = \frac{\pi}{2}, \delta_{\mathrm{l}}\right)\mathbf{E}(\mathrm{A}), \tag{44}$$

where $D$ is the AE-to-FE length ratio (here, we assume that they are made of the same material), $R(\beta)$ is the matrix of rotation through an angle $\beta$, and the matrices $F$ and $L_2$ are defined by formulas (4) and (18). The linear birefringence phase difference in the FEs that rotate the polarization through the angle $\Phi = \pi/8$ ($\delta_{\mathrm{c}} = \pi/4$) is equal to $\delta_{\mathrm{l}}/2$ in this case, i.e., for all FIs shown in Fig. 1 and Fig. 6, the value of $\delta_{\mathrm{l}}$ is the total phase increment of linear birefringence over the whole length of the magnetoactive medium. This permits a correct comparison of different FIs.

In the approximation defined by inequality (19), substituting expressions (42)–(44) in (15) gives expressions for $\gamma_{\mathrm{L,R,A}}$, whence it is easy to obtain that for $D = \sqrt{8}/\pi$ and the optimal values of the angles

$$\beta_{\mathrm{L}} = \beta_{\mathrm{opt\,L}} = \frac{\pi}{8}, \quad \beta_{\mathrm{R}} = \beta_{\mathrm{opt\,R}} = \frac{3\pi}{8}, \quad \beta_{\mathrm{A}} = \beta_{\mathrm{opt\,A}} = \frac{3\pi}{8}, \tag{45}$$

the quantities $\gamma_{\mathrm{L,R,A}}$ become proportional to the fourth power of $\delta_{\mathrm{l}}$, while $\gamma_p$ in (23) is proportional to the square of $\delta_{\mathrm{l}}$. In view of inequality (19), this is an indication that the depolarization in all new FIs (see Fig. 6) is much smaller than in the traditional FI (see Fig. 1). For optimal $\beta$ values, we obtain [47, 65]

$$\gamma_{\mathrm{L}} = 8A_{\mathrm{c}}(b^2 - a^2)p^4\xi^2, \quad \gamma_{\mathrm{R}} = 6A_{\mathrm{c}}a^2p^4\left(1 + \frac{2}{3}\xi^2 + \xi^4\right), \quad \gamma_{\mathrm{A}} = 6A_{\mathrm{c}}c^2p^4\left(1 + \frac{2}{3}\xi^2 + \xi^4\right), \tag{46}$$

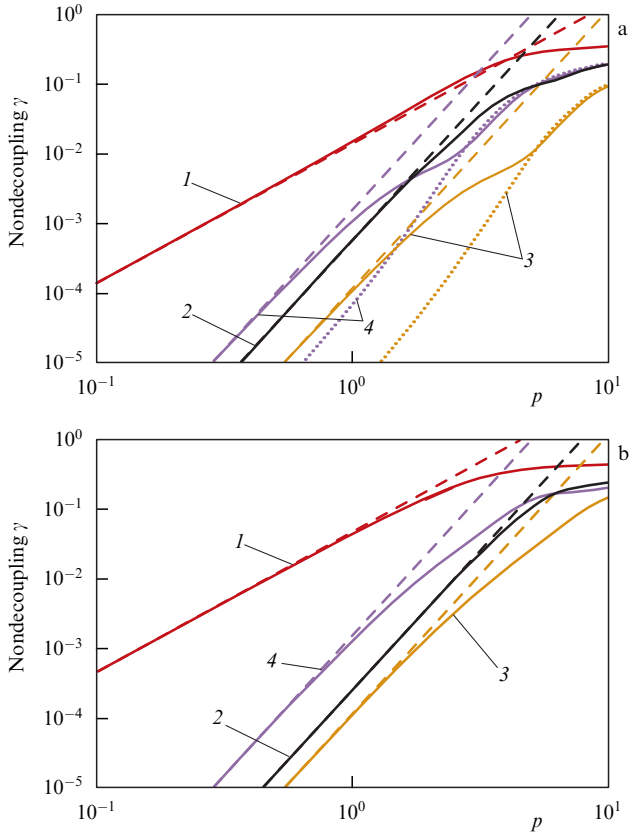


**Figure 7.** Dependences $\gamma(p)$ for the TGG crystal of the orientation (a) [001] and (b) [111]: $\gamma_p$ for a traditional FI (curves *1*), $\gamma_{\mathrm{L}}$ for a $\lambda/2$ FI (curves *2*), $\gamma_{\mathrm{R}}$ for an FI with RR (curves *3*), and $\gamma_{\mathrm{A}}$ for an FI with AE (curves *4*). Dashed lines stand for the dependences defined by formulas (23) and (46), solid lines stand for the data of numerical calculations, and dotted lines stand for the 73° RR rotation angle.

where $a = (\pi - 2\sqrt{2})/8$, $b = (2 - \sqrt{2})/4$, and $c = (\pi - 2)/8$. For $0.76 < \xi < 1.3$, the expression for $\gamma_{\mathrm{L}}$ has a different form (see Ref. [98]).

Therefore, the nondecoupling $\gamma_{\mathrm{L,R,A}}$ of all three new FIs (as with traditional FIs) is determined by only two parameters: $p$ and $\xi$. For a super-Gaussian beam, formulas (46) remain valid for any $m$ if $A_{\mathrm{c}}$ is replaced with $A_{\mathrm{c}}(m)$ (see Table 2).

Figure 7 shows the results of numerical integration, which does not require approximation (19), for all four FI types with a TGG crystal with [001] and [111] orientations. We can see from the figure that the data of exact calculations deviate significantly from formulas (23) and (46) only for large $p$. In the cases of practical interest ($\gamma < 0.01$), formulas (23) and (46) can be used.

We also see from Fig. 7 that an FI with an RR provides the smallest nondecoupling, which underlies its wider acceptance. Furthermore, as shown in Ref. [65], when FEs have different lengths and different directions of crystallographic axes relative to the polarization of the incident radiation (the angle $\theta$ in Fig. 2), it is possible to find the angle of polarization rotation in the RR such that the nondecoupling is much weaker. This angle depends on the FE material properties. As shown theoretically for TGG monocrystals of the [001] orientation, the optimal angle is equal to about 73° rather than to 67.5°. This was experimentally confirmed in Ref. [68] (see below).

The nondecoupling of a $\lambda/2$ FI (and more so of an FI with an AE) is several times greater than the nondecoupling of an FI with an RR (see Fig. 7). However, the former also offers an advantage: different directions of the magnetic field in $\lambda/2$ FIs, which permits placing both FEs in the maximum field domains and shortening their length $L$ [105], and the magnitude of $\gamma_{\rm L}$ being proportional to $L^4$. Moreover, for high $\xi$, as is clear from formulas (46), $\gamma_{\rm L}$ is proportional to $\xi^2$ rather than $\xi^4$, like $\gamma_{\rm R,A}$, which offers an advantage when crystals with a high $\xi$ are used.

The FIs with an AE also offer advantages. First, there is the possibility of upgrading traditional FIs (see Fig. 1) without changing the magnetic system and the FE. Second, for the material of an AE, it is possible to choose another, not necessarily magnetoactive, optical material, which can be selected depending on the availability, cost, material constants, etc. The significant difference in the characteristics of FE and AE materials permits improving the compensation. This problem was theoretically considered in Ref. [66], where the parameters responsible for the compensation were determined. As is shown theoretically and experimentally in Ref. [66], by selecting a material with a negative $\xi$ value or the difference $\pi_{11} - \pi_{12}$ of opposite sign, it is possible to exclude a reciprocal polarization rotator from the FIs with an AE, and by selecting a material with a negative $P$, it is possible to additionally weaken the focal power of the thermal lens. For instance, the $CaF_2$ crystal has both of these properties: $\xi < 0$ and $P < 0$. Because pure $CaF_2$ has a very low absorption at a wavelength of 1 μm, it is expedient to use $Sm^{2+}$-doped $CaF_2$ (0.01 of the weight percent of $SmF_2$) [68].

With (39) and (40), we can see from formulas (46) that [001] is the orientation of choice when using TGG ($\xi = 2.25$) for a $\lambda/2$ FI and traditional FIs. In FIs with an RR and FIs with an AE, the depolarization is practically the same for crystals of [001] and [111] orientations and ceramics. The problem of an FI with RR with an arbitrary crystal orientation was considered in Ref. [54], where [001] and [111] were shown to be the orientations of choice. The [111] orientation does not require the mutual alignment of FEs, which makes it more convenient in practice. At the same time, the [001] orientation, unlike [111], permits an additional lowering of the nondecoupling due to the use of a 73° rotator, which requires an exact alignment of both FEs.

The power loss in the spatial polarization mode for new FIs is calculated by the procedure described in Sections 2.2 and 2.4 [51]. As in the case of traditional FIs, the total loss $\gamma_{\rm total} = \gamma_1 + \gamma_{\rm a} + \gamma_{\rm i}$ is the sum of three terms, which are independent of the beam radius $r_0$ and are proportional to the square of $p$ or $p_{\rm i}$. The formulas for these terms are given in Table 1 below. As would be expected, the isotropic loss $\gamma_{\rm i}$, $\gamma_S$, and $\gamma_M$ for an FI with an AE are $(1 + \sqrt{8}/\pi)^2$ times greater than for other FIs, because the AE introduces its phase distortions. But when the AE is made of a material with $P$ of the opposite sign, the total phase distortion are smaller, i.e., the thermal lens is compensated simultaneously with the depolarization compensation (see Section 3.3).

As pointed out in Section 2.5, the polarization of radiation transmitted through a nonuniformly heated FE depends on the magnetic field distribution along the $z$ axis. In the foregoing, we assumed that $B(z) = \text{const}$. When $B(z) \neq \text{const}$, a term proportional to $p^2$ appears in expression (46) for depolarization in the new FIs. Using (36) and the known expressions for the transformation of $\chi$ in the optical elements with constant parameters along the $z$ axis (see, e.g., Ref. [97]), it is possible to calculate the value of $\chi$ sequentially in all elements of the FI. Assuming that the resultant $\chi$ is known, we find the following expressions for the depolarization in the new FIs, up to terms of the order of $\delta_1^4$:

$$\Gamma_{\rm L} = \left(\frac{\delta_1}{2L}\right)^2 \left[\int_0^{L/2} \sin\left(2\Psi + 2\theta + \frac{\pi}{4} - \int_0^z \Delta_{2\rm L}\,{\rm d}y\right){\rm d}z - \int_0^{L/2} \sin\left(2\Psi + 2\theta + \int_0^z \Delta_{1\rm L}\,{\rm d}y\right){\rm d}z\right]^2, \tag{47}$$

$$\Gamma_{\rm R} = \left(\frac{\delta_1}{2L}\right)^2 \left[\int_0^{L/2} \sin\left(2\Psi + 2\theta + \int_0^z \Delta_{1\rm R}\,{\rm d}y\right){\rm d}z - \int_0^{L/2} \sin\left(2\Psi + 2\theta + \int_0^z \Delta_{2\rm R}\,{\rm d}y\right){\rm d}z\right]^2, \tag{48}$$

$$\Gamma_{\rm A} = q^2 + 2qs\cos\left(\frac{5\pi}{16}\right) + s^2, \tag{49}$$

where

$$q = \frac{\delta_1}{2L}\int_0^L \sin\left(2\Psi - \delta_{\rm c}(z)\right){\rm d}z, \qquad s = \frac{\sqrt{2}\,\delta_1}{\pi}\sin\left(2\Psi - \frac{3\pi}{16}\right),$$

$\Delta(z) = |2VB(z)|$, and the indices 1 and 2 refer to the first and second FEs. For an arbitrary distribution of $B(z)$, expressions (47)–(49) permit calculating the nondecoupling caused by the longitudinal nonuniformity of the magnetic field. For $B(z) = \text{const}$, the right-hand sides of Eqns (47)–(49) vanish. Furthermore, it is easy to show that they also vanish in Eqns (47) and (48) when

$$\Delta_{1\rm L}(z) = \Delta_{2\rm L}\left(\frac{L}{2} - z\right), \qquad \Delta_{1\rm R}(z) = \Delta_{2\rm R}(z). \tag{50}$$

The second condition in (50) signifies that the magnetic field in the second FE repeats the field in the first one, which, as a rule, in not fulfilled in practice, because the magnetic field is usually reflection symmetric. In an experiment with an FI with an RR, we observed a significant increase in depolarization when condition (50) was not satisfied (cf. the filled and empty squares in Fig. 8a).

### 3.2 Depolarization compensation. Experimental results

The efficiency of depolarization compensation in a $\lambda/2$ FI and an FI with an RR was first verified experimentally for a glass FE in Ref. [49]. Figure 8a shows experimental data and theoretical curves. For a high power, the depolarization is determined primarily by thermal effects. The quantitative agreement of experimental data with the theoretical ones for $\gamma_p$ (i.e., ignoring the temperature dependence of the Verdet constant) confirms the prediction of the theory that it is precisely the photoelastic effect that determines the isolation ratio for a high average radiation power. In particular, it is clearly seen that the nondecoupling $\gamma$ is proportional to the fourth power of $p$ for a $\lambda/2$ FI and an FI with an RR. An analysis of the transverse structure of depolarized radiation for all three scenarios (see the images in the right part of Fig. 8a) also confirmed this fact [49].

Most important for lasers with a high average power are not magnetoactive glasses but TGG crystals, for which the efficiency of an FI with an RR was also experimentally confirmed in 2000 [52]. For a power up to 73 W, the nondecoupling was under $3 \times 10^{-5}$ and the thermal effects

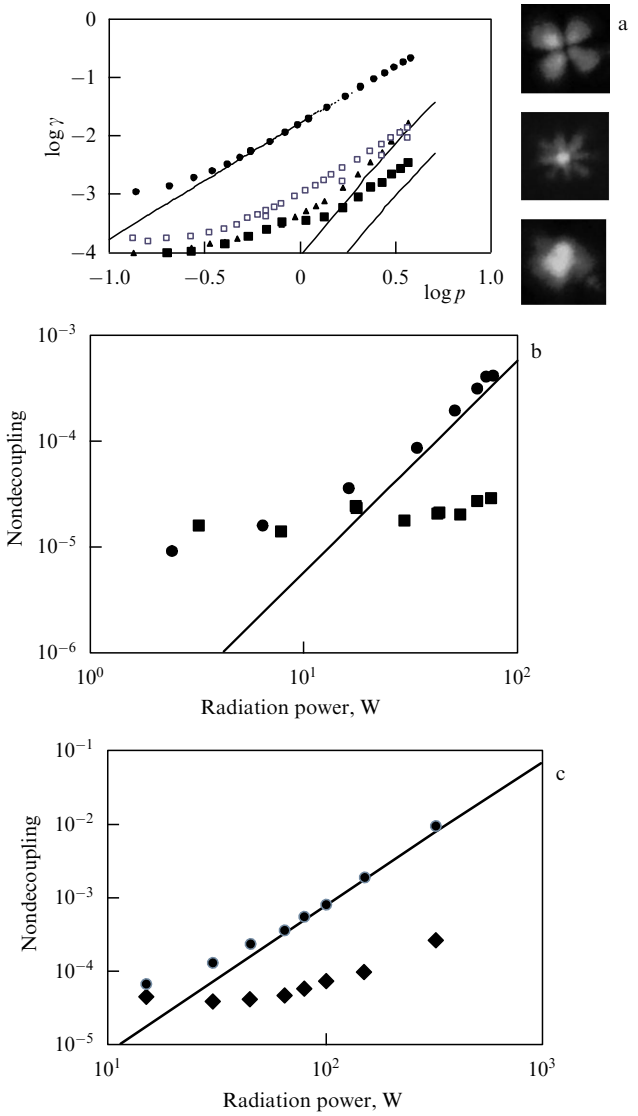


**Figure 8.** Theoretical (solid lines) and experimental (symbols) dependences of the nondecoupling for an FI with an FE of glass (a) [49] and TGG (b) [52], (c) [65]. The circles stand for a traditional FI (see Fig. 1), triangles for an $\lambda/2$ FI (Fig. 6a), squares for an FI with a RR (Fig. 6b), and diamonds for an FI with an AE (Fig. 6c). Empty circles in Fig. 8a show the nondecoupling under violation of the symmetry of the longitudinal magnetic field distribution (50). Shown in the right part of Fig. 8a are the transverse nondecoupling distributions for a traditional FI (top), a $\lambda/2$ FI (middle), and an FI with an RR (bottom).

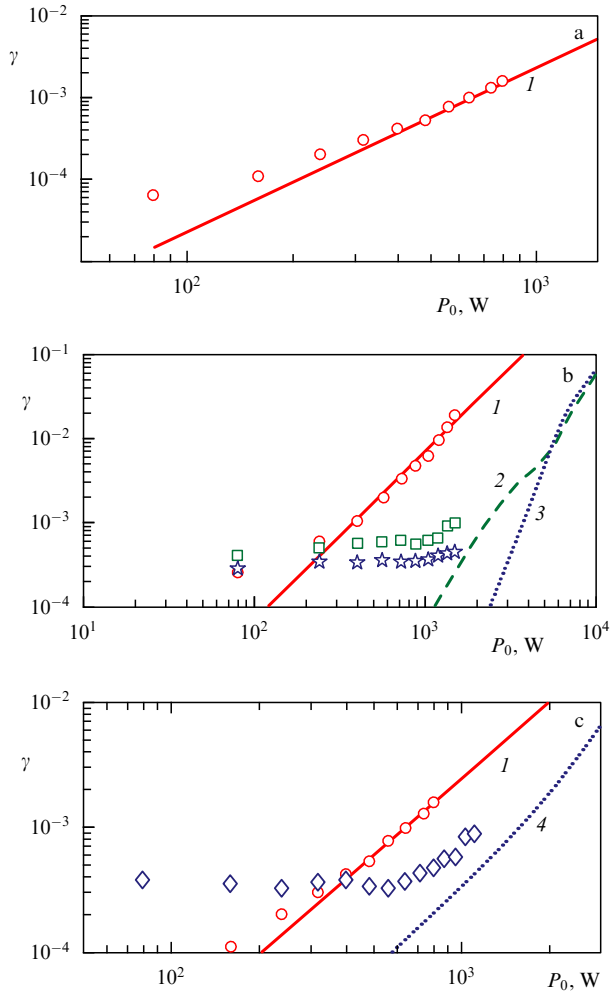


**Figure 9.** Experimental dependences of nondecoupling on the radiation power $P_0$ for (a) a traditional FI, $\gamma_p$ (circles), (b) an FI with an RR, $\gamma_R$, for a 67.5° RR (squares), a 73° RR (stars), and (c) an FI with an AE, $\gamma_A$ (diamonds) [68]. Also shown in Figs 9b and 9c are the data obtained for the traditional FI (circles) under the same experimental conditions. The curves represent the data of theoretical calculations for a traditional FI (curves *1*), an FI with a 67.5° RR (curve *2*), an FI with a 73° RR (curve *3*), and an FI with an AE (curve *4*).

were hardly observable (Fig. 8b). An FI with an AE was first realized in Ref. [65], in which a 36-fold decrease in $\gamma$ compared with a traditional FI was demonstrated for a power of 330 W (Fig. 8c).

FIs with an RR and FIs with an AE have been studied in many papers [49, 52, 62, 63, 65, 66, 68, 71, 106–110] for the laser power up to 1.5 kW (see Table 3). Figure 9 shows experimental data for a power above 1 kW [68]. As in Figs 3 and 8, for a low power, $\gamma$ is determined by 'cold' FE depolarization, the contrast ratio of the polarizers in use, and the nonuniformity of the magnetic field; as the power increases, $\gamma$ increases and tends to theoretical dependences (46), represented by solid lines in Fig. 9.

The parameter $p$ depends not only on the radiation power but also on the FE length $L$, which is in turn inversely proportional to the magnetic field. The problem of increasing the magnetic field is discussed at length in Section 4.3; here, we only note that increasing the FE diameter inevitably leads to a decrease in the magnetic field and hence an increase in $\gamma$. In this connection, we note FIs with RRs with apertures of 30 mm [68] and 40 mm [106], in which the record high aperture of TGG crystals is combined with minimal nondecoupling values.

In the foregoing, we disregarded an increase in the average FE temperature, because its only negative consequence is a decrease in the polarization rotation angle due to the $V(T)$ dependence. For a power of 1 kW, the characteristic decrease amounts to 3–5° [68]. This is not essential for the isolation ratio, because by aligning the $\lambda/2$ plate or the polarizer it is possible in practice to minimize $\gamma_V$ [the second term in expression (21)] for any heating. In this case, only the forward-passage depolarization $\gamma_1$ shows an increase. Or, conversely, to preserve the $\gamma_1$ value, the FE length $L$ is increased such that the polarization rotation angle is equal to 45° in the heated state. The nondecoupling $\gamma_p$ increases in this case, because it is proportional to $L^2$. Reducing the heating of the FE requires a good thermal contact; a very

high power requires active cooling by water [106] or a Peltier element [111]. There are FIs that are insensitive to a temperature increase owing to a complex optical scheme with different directions of the magnetic field [112], a special configuration of the magnetic field, and special material of the FE holder [113]. It is noteworthy that the problem of the average temperature increase in FEs is more acute for FIs operating in a vacuum. For instance, the FIs for the LIGO and Virgo gravitational wave detectors are described at length in Refs [107, 114, 115].

Thus, the maximum laser power reached to date for FIs with an AE is $P_{\max} = 1.1$ kW; the $P_{\max}$ value for FIs with an RR is approaching 3 kW.

### 3.3 Thermal lens compensation

The temperature distribution in an optical element and hence the phase distribution of an aberrated laser beam are close to parabolic. A significant part of phase distortions can be compensated with an ordinary (parabolic) lens or a telescope (element *6* in Fig. 5), which introduce additional curvature into the wavefront [51]. (In what follows, this method is referred to as telescope compensation and the corresponding loss is denoted by the subscript TC.) The focal length $f$ of the compensating lens [93] depends on the parameter that we choose to increase: the overlap integral or the Strehl number (the parameter $M^2$ is independent of the parabolic beam phase). In the former case, we minimize $\gamma_{\rm i}$ and in the latter case, $\gamma_S$; as a result, we obtain

$$f_{\rm i} = -A_F \frac{kr_0^2}{p_{\rm i}}\,, \qquad f_S = -A_{FS} \frac{kr_0^2}{p_{\rm i}}\,. \tag{51}$$

For a Gaussian beam, $f_{\rm i}$ differs from $f_S$ by a factor of 1.5, and $f_{\rm i}$ coincides up to a sign with the focal length $F$ of the thermal lens, Eqn (53) (see Table 2). After minimization, we obtain [93]

$$\gamma_{\rm i,TC} = A_{\rm i,TC}\, p_{\rm i}^2\,, \qquad \gamma_{S,\rm TC} = A_{S,\rm TC}\, p_{\rm i}^2\,. \tag{52}$$

By telescope compensation, the isotropic loss $\gamma_{\rm i}$ can be decreased by the factor $A_{\rm i}/A_{\rm i,TC} \approx 15$ and $\gamma_S$ by the factor $A_S/A_{S,\rm TC} \approx 8$. The compensation is more efficient for super-Gaussian beams than for Gaussian ones (see Table 2). For rectangular beams, the thermal phase is strictly parabolic and the thermal lens is fully compensated: $A_{\rm i,TC}(m=\infty) = A_{S,\rm TC}(m=\infty) = 0$.

The authors of [55, 116] proposed and experimentally studied an adaptive compensation (AC) of the thermal lens in an FI. Placed in front of polarizer *1* is an absorber (see Fig. 5) whose parameters are selected in such a way that the thermal lens has the same amplitude and shape as in the FI, but is negative, $P_{\rm AC} < 0$ (for the majority of magnetoactive materials, it is positive). As shown in Ref. [55], the diffraction beam spreading between the absorber and the FI may be ignored when the distance between them is short. The isotropic loss is then fully compensated: $\gamma_{\rm i,AC} = \gamma_{S,\rm AC} = \gamma_{M,\rm AC} = 0$. The adaptive compensation offers two indubitable advantages: there is no necessity for alignment when the laser power is changed, and it is possible to achieve a higher compensation accuracy. But a significant drawback of adaptive compensation is that the photoelastic effect in the absorber results in additional anisotropic distortions and consequently in an increase in $\gamma_1$ and $\gamma_{\rm a}$ (see Fig. 5).

Therefore, the telescope compensates isotropic distortions with a lower efficiency, but at the same time it does not lead to an additional increase in the losses $\gamma_1$ and $\gamma_{\rm a}$. Adaptive compensation nullifies isotropic distortions but increases the losses $\gamma_1$ and $\gamma_{\rm a}$ caused by the photoelastic effect in the absorber. Analytic expressions for $\gamma$ borrowed from Refs [51, 93, 117] are given in Table 1. These formulas hold when $\theta = \theta_{\rm opt}$ and condition (19) is satisfied. The parameter $p_{\rm AC}$ is defined by formula (12), in which all material constants correspond to the absorber.

The key absorber parameter is the ratio $P_{\rm AC}/Q_{\rm AC}$, and the greater this ratio, the better. In particular, when this ratio is much greater than the corresponding ratio for a magnetoactive crystal, the additional increase in $\gamma_1$ and $\gamma_{\rm a}$ may be disregarded, because the only drawback of adaptive compensation vanishes. Using the most popular glass FK51 with negative $P_{\rm AC}$, the authors of Ref. [117] could efficiently compensate for the thermal lens; but because of the small value $P_{\rm FK51}/Q_{\rm FK51} = 2.8$, the uncompensated astigmatism turned out to be too strong.

The photoelastic effect can be completely eliminated if the absorber is chosen as a crystal with natural birefringence, in the background of which the induced birefringence can be ignored [8], i.e., $p_{\rm AC} = 0$. DKDP (deuterated potassium dihydrogen phosphate) seems to be the candidate of choice. Figure 10 shows the two-dimensional phase distributions obtained in Ref. [118] using a 5.5 mm thick DKDP crystal. For a radiation power of 45 W, it was experimentally demonstrated that the thermally induced loss $\gamma_{\rm i}$ in a Gaussian beam decreased from 26% to 0.5%. DKDP crystals are widely used for compensating the thermal lens in FIs, in particular, in FIs with an RR used in interferometer gravitational wave detectors [107, 115].

We note that DKDP has poor thermal characteristics and is difficult to use for an average power above 1 kW. As shown in Refs [119, 120], the thermally induced depolarization can be completely eliminated in crystals with a negative $\xi$ value by optimizing its orientation. An example is provided by the $CaF_2$ crystal with $\xi = -0.47$ [120]; its optimal orientation is

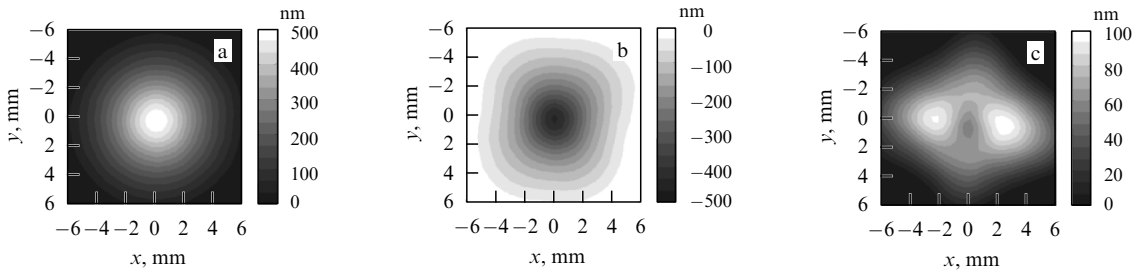


**Figure 10.** (Color online.) Measured [118] spatial distributions of the beam phase after (a) an FI, (b) DKDP, and (c) FI and DKDP.

**Table 1.** Expressions for the nondecoupling $\gamma_p$ and $\gamma_V$, the polarization $\gamma_1$, the anisotropic $\gamma_a$ and isotropic $\gamma_i$ loss in the forward passage, a decrease in the Strehl number $\gamma_S$, and an increase in the $M^2$ parameter $\gamma_M$. Constants $A$ are given in Table 2.

| Compensation method | | Nondecoupling | Traditional FI (see Fig. 1) | FI with depolarization compensation | | |
|---|---|---|---|---|---|---|
| | | | | $\lambda/2$ FI (Fig. 6a) | FI with RR (Fig. 6b) | FI with AE (Fig. 6c) |
| Without thermal lens compensation | | $\gamma_V$ | $A_V p_V^2$ | $A_V p_V^2$ | $A_V p_V^2$ | $A_V p_V^2$ |
| | | $\gamma_p$ | $A_p p^2$ if $\lvert\xi\rvert \geqslant 1$ | $A_c\left(\frac{(4-\pi)(4+\pi-\sqrt{32})}{8}\right)p^4\xi^2$ if $\xi < 0.76$ and $\xi > 1.3$ | $6A_c\left(\frac{\pi-\sqrt{8}}{8}\right)^2 p^4\left(1+\frac{2}{3}\xi^2+\xi^4\right)$ | $6A_c\left(\frac{\pi-2}{8}\right)^2 p^4\left(1+\frac{2}{3}\xi^2+\xi^4\right)$ |
| | | | $A_p p^2\xi^2$ if $\lvert\xi\rvert < 1$ | | | |
| | | $\gamma_1$ | $A_p p^2\xi^2$ if $\lvert\xi\rvert \geqslant 1$ | $\left(2-\frac{\pi}{2}\right)A_p p^2(\xi^2+1)$ if $\xi < 0.76$ and $\xi > 1.3$ | $A_p(2-\sqrt{2})p^2$ if $\lvert\xi\rvert \geqslant 1$ | $A_p p^2$ if $\lvert\xi\rvert \geqslant 1$ |
| | | | $A_p p^2$ if $\lvert\xi\rvert < 1$ | | $A_p(2-\sqrt{2})p^2\xi^2$ if $\lvert\xi\rvert < 1$ | $A_p p^2\xi^2$ if $\lvert\xi\rvert < 1$ |
| | | $\gamma_a$ | $A_p p^2$ if $\lvert\xi\rvert \geqslant 1$ | $O(p^4)$ | $A_p(2-\sqrt{2})p^2\xi^2$ if $\lvert\xi\rvert \geqslant 1$ | $A_p p^2(2\xi^2+1)$ if $\lvert\xi\rvert \geqslant 1$ |
| | | | $A_p\xi^2$ if $\lvert\xi\rvert < 1$ | | $A_p(2-\sqrt{2})p^2$ if $\lvert\xi\rvert < 1$ | $A_p p^2(\xi^2+2)$ if $\lvert\xi\rvert < 1$ |
| | | $\gamma_i$ | $A_i p_i^2$ | $A_i p_i^2$ | $A_i p_i^2$ | $A_i p_i^2(1+\sqrt{8}/\pi)^2$ |
| | | $\gamma_S$ | $A_S p_i^2$ | $A_S p_i^2$ | $A_S p_i^2$ | $A_S p_i^2(1+\sqrt{8}/\pi)^2$ |
| | | $\gamma_M$ | $A_M p_i^2$ | $A_M p_i^2$ | $A_M p_i^2$ | $A_M p_i^2(1+\sqrt{8}/\pi)^2$ |
| With thermal lens compensation | Telescope compensation | $\gamma_{1,\mathrm{TC}}$ | $\gamma_1$ | $\gamma_1$ | $\gamma_1$ | $\gamma_1$ |
| | | $\gamma_{a,\mathrm{TC}}$ | $\gamma_a$ | $\gamma_a$ | $\gamma_a$ | $\gamma_a$ |
| | | $\gamma_{i,\mathrm{TC}}$ | $A_{i,\mathrm{TC}}p_i^2$ | $A_{i,\mathrm{TC}}p_i^2$ | $A_{i,\mathrm{TC}}p_i^2$ | $A_{i,\mathrm{TC}}p_i^2(1+\sqrt{8}/\pi)^2$ |
| | | $\gamma_{S,\mathrm{TC}}$ | $A_{S,\mathrm{TC}}p_i^2$ | $A_{S,\mathrm{TC}}p_i^2$ | $A_{S,\mathrm{TC}}p_i^2$ | $A_{S,\mathrm{TC}}p_i^2(1+\sqrt{8}/\pi)^2$ |
| | | $\gamma_{M,\mathrm{TC}}$ | $\gamma_M$ | $\gamma_M$ | $\gamma_M$ | $\gamma_M$ |
| | Adaptive compensation | $\gamma_{1,\mathrm{AC}}$ | $\gamma_1 + A_p p_{\mathrm{AC}}^2\pi^2/8$ | $\gamma_1 + A_p p_{\mathrm{AC}}^2\pi^2/8$ | $\gamma_1 + A_p p_{\mathrm{AC}}^2\pi^2/8$ | $\gamma_1 + A_p p_{\mathrm{AC}}^2\pi^2/8$ |
| | | $\gamma_{a,\mathrm{AC}}$ | $\gamma_a + \pi^2 A_p p_{\mathrm{AC}}^2/8 + \pi A_p\xi p p_{\mathrm{AC}}/\sqrt{8}$ | | | |
| | | $\gamma_{i,\mathrm{AC}}$ | 0 | 0 | 0 | 0 |
| | | $\gamma_{S,\mathrm{AC}}$ | 0 | 0 | 0 | 0 |
| | | $\gamma_{M,\mathrm{AC}}$ | 0 | 0 | 0 | 0 |

**Table 2.** Constants $A$ for different $m$. $A_x = A_x(m=1)$ for any subscript $x$.

| Constants | Super-Gaussian distribution index $m$ | | | |
|---|---|---|---|---|
| | 1 | 2 | 8 | $\infty$ |
| $A_V(m) = \frac{m}{\Gamma(1/m)}\int_0^\infty \frac{u^2(t)\,\mathrm{d}t}{\exp t^m} - \frac{m^2}{\Gamma^2(1/m)}\left[\int_0^\infty \frac{u(t)\,\mathrm{d}t}{\exp t^m}\right]^2 = A_\mathrm{i}(m)$ | 0.067 | 0.039 | 0.023 | 1/36 |
| $A_p(m) = \frac{m^3}{\pi^2\Gamma^3(1/m)}\int_0^\infty \left[\int_0^t \mathrm{d}z \int_0^z \frac{\mathrm{d}t}{\exp t^m}\right]^2 \frac{\mathrm{d}t}{t^2 \exp t^m}$ | 0.0139 | 0.0113 | 0.0088 | 0.0085 |
| $A_\mathrm{c}(m) = \frac{m^5}{\pi^4\Gamma^5(1/m)}\int_0^\infty \left[\int_0^t \mathrm{d}z \int_0^z \frac{\mathrm{d}t}{\exp t^m}\right]^4 \frac{\mathrm{d}t}{t^4 \exp t^m}$ | $4.31 \times 10^{-4}$ | $2.72 \times 10^{-4}$ | $1.5 \times 10^{-4}$ | $1.28 \times 10^{-4}$ |
| $A_\mathrm{i}(m) = \frac{m}{\Gamma(1/m)}\int_0^\infty \frac{u^2(t)\,\mathrm{d}t}{\exp t^m} - \frac{m^2}{\Gamma^2(1/m)}\left[\int_0^\infty \frac{u(t)\,\mathrm{d}t}{\exp t^m}\right]^2 = A_V(m)$ | 0.067 | 0.039 | 0.023 | 1/36 |
| $A_S(m) = \frac{m}{\Gamma(1/m)}\int_0^\infty \frac{u^2(t\sqrt[m]{2})\,\mathrm{d}t}{\exp t^m} - \frac{m^2}{\Gamma^2(1/m)}\left[\int_0^\infty \frac{u(t\sqrt[m]{2})\,\mathrm{d}t}{\exp t^m}\right]^2$ | 0.127 | 0.062 | 0.027 | 1/36 |
| $A_M(m) = \frac{m}{\Gamma^2(1/m)}\int_0^\infty \left[\int_0^t \frac{\mathrm{d}y}{\exp y^m}\right]^2 \exp(-t^m)\,\frac{\mathrm{d}t}{t} - \frac{\Gamma^2(1/m)}{4m^2\Gamma(2/m)}$ | 0.038 | 0.0072 | $8 \times 10^{-5}$ | 0 |
| $A_{\mathrm{i,TC}}(m) = A_\mathrm{i}(m) - \frac{m^2\Gamma^2(2/m)}{\Gamma^2(1/m)\left(\Gamma(1/m)\Gamma(3/m) - \Gamma^2(2/m)\right)} \times \left[\int_0^\infty \frac{u(t)\left\{1 - t\Gamma(1/m)/\Gamma(2/m)\right\}\mathrm{d}t}{\exp t^m}\right]^2$ | $4.4 \times 10^{-3}$ | $5.1 \times 10^{-4}$ | $2.5 \times 10^{-6}$ | 0 |
| $A_{S,\mathrm{TC}}(m) = A_S(m) - \frac{m^2\Gamma^2(2/m)}{\Gamma^2(1/m)\left(\Gamma(1/m)\Gamma(3/m) - \Gamma^2(2/m)\right)} \times \left[\int_0^\infty \frac{u(t\sqrt[m]{2})\left\{1 - t\Gamma(1/m)/\Gamma(2/m)\right\}\mathrm{d}t}{\exp t^m}\right]^2$ | 0.016 | 0.00177 | $7.96 \times 10^{-6}$ | 0 |
| $A_F(m) = \frac{2\Gamma(2/m)}{\Gamma(1/m)}$ | 2 | 1.13 | 0.96 | 1 |
| $A_{F,\mathrm{i}}(m) = \frac{\Gamma(1/m)\Gamma(3/m) - \Gamma^2(2/m)}{2m\Gamma(2/m)}\left[\int_0^\infty \frac{u(t)\left\{1 - t\Gamma(1/m)/\Gamma(2/m)\right\}\mathrm{d}t}{\exp t^m}\right]^{-1}$ | 2 | 1.08 | 0.95 | 1 |
| $A_{F,S}(m) = \sqrt[m]{2}\,\frac{\Gamma(1/m)\Gamma(3/m) - \Gamma^2(2/m)}{2m\Gamma(2/m)}\left[\int_0^\infty \frac{u(t\sqrt[m]{2})\left\{1 - t\Gamma(1/m)/\Gamma(2/m)\right\}\mathrm{d}t}{\exp t^m}\right]^{-1}$ | 3 | 1.22 | 0.95 | 1 |

close to [111]. Using this material as the absorber, it is possible to ensure that $\gamma_\mathrm{i} = \gamma_S = \gamma_M = 0$ without increasing either $\gamma_1$ or $\gamma_\mathrm{a}$, as with telescope compensation.

Furthermore, the thermal lens can be compensated by using two FEs with $P$ of opposite sign. $LiTbF_4$ crystals, whose Verdet constant is approximately the same as in TGG [121] and $\mathrm{d}n/\mathrm{d}T < 0$ [122], may be useful for this purpose.

## 4. Suppression of thermal effects in Faraday isolators

By suppression of distortions, we mean their decrease with the FI scheme depicted in Fig. 1 preserved. In Section 4.1, we consider a cryogenic FI in which the suppression is achieved by cooling to 77 K. In Sections 4.2 and 4.3, we discuss the problem of an alternative to the TGG crystals, the figures of merit of magnetoactive media, and directions in the search for new materials. In Sections 4.4 and 4.5, we consider the methods of thermal effect suppression like enhancement of the magnetic field and the use of non-rod-shaped geometry of heat removal from an FE.

### 4.1 Cryogenic Faraday isolator

The cooling of FIs was first proposed in [123] back in 1967 for shortening the FE: high-quality FEs were nonexistent at that time, while cooling results in a significant increase in the Verdet constant $V$ and, accordingly, in shortening the FE length $L$. After the solution of the FE quality problem, this idea was abandoned for lack of need. The authors of Ref. [124] proposed cooling FIs to liquid-nitrogen temperature to weaken the thermal effects and make FIs for lasers with a high average power.

The Verdet constant of TGG crystals is, to a high accuracy, inversely proportional to the temperature [125, 126]. The same dependence also holds for TGG ceramics [127]. This permits decreasing $L$ by a factor of 3.8 by cooling to 77 K. Furthermore, all thermooptical constants become smaller under cooling: $Q$ decreases by a factor of 5.7 [128], $P$

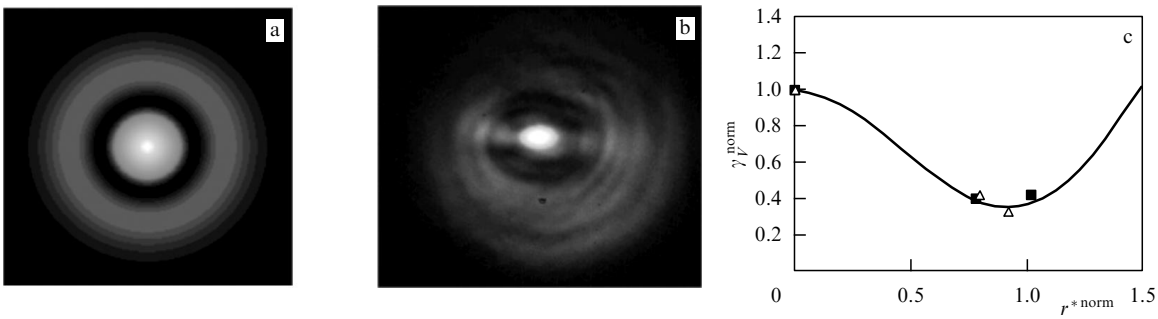


**Figure 11.** (Color online.) Theoretical (a) and experimental (b) distributions $\Gamma_V(r,\varphi)$ for $r^* = r_{\rm opt} \approx 0.92 r_0$. (c) Dependence $\gamma_V(r^*/r_0)$ normalized to $\gamma_V(r^* = 0)$ for $P_0 = 530$ W (squares) and 765 W (triangles) [128].

by a factor of 6.8 [128], and $\xi$ by a factor of 1.7 [129]. The thermal conductivity is virtually unchanged for TGG crystals grown from melt and increases twofold for the crystals grown from flux [130]. The absorption at a temperature of 80 K measured in Ref. [128] was twice the room-temperature absorption. By substituting these values in formulas (12) and (32), we obtain a significant decrease in the parameters $p$ and $p_{\rm i}$, which determine the polarization distortions and thermal lens induced by the photoelastic effect:

$$\frac{p(273\ {\rm K})}{p(77\ {\rm K})} = 10.8\,, \qquad \frac{p_{\rm i}(273\ {\rm K})}{p_{\rm i}(77\ {\rm K})} = 12.3\,. \tag{53}$$

As is evident from formulas (12) and (32), the decrease in these parameters permits increasing the radiation power $P_0$ by the same factor. The decrease in $\xi$ also decreases some distortions (see Table 1). Furthermore, the shortening of an FE permits organizing longitudinal heat removal, for instance, with a crystal of yttrium aluminum garnet (YAG) or sapphire [128, 131], which reduces thermal effects (for more details, see Section 4.4).

At the same time, as is clear from expressions (24) and (25), the nondecoupling $\gamma_V$, which is caused by the temperature dependence $V = {\rm const}/T$, increases significantly because $V^{-1}({\rm d}V/{\rm d}T) = -1/T$, to become 3.8 times greater. For TGG at $T = 77$ K, we obtain $L^* \approx 13$ mm from formula (26), which is comparable to or even longer than the FE length in cryogenic FIs. Therefore, in cryogenic isolators, the condition $\gamma_V \ll \gamma_p$ can be violated. Under the condition $L \ll L^*$, the thermally induced depolarization was first observed in Ref. [128]. Figures 11a and 11b show the theoretical and measured spatial nondecoupling distributions $\Gamma(r,\varphi)$ when the photoelastic effect can be completely neglected, i.e., the first term omitted in formula (20). The dark ring corresponds to the radius $r = r^*$ at which the rotation angle of the polarization plane is exactly equal to $\pi/4$. As mentioned in Section 2.2, it is possible to select the value of $r^*$ that minimizes the integral nondecoupling $\gamma_V$. Constructed in Fig. 11c is the $\gamma_V(r^*)$ dependence, which has a minimum for $r^* = r_{\rm opt} \approx 0.92 r_0$, as predicted in Ref. [98].

The methods of depolarization compensation discussed in Section 3.1 permit decreasing $\gamma_p$, but they in no way affect $\gamma_V$. To compensate $\gamma_V$, a magnetic system was made in [132] in which the central magnetic field exceeded the peripheral one. In the same way, it is possible to compensate the effect of nonuniform FE magnetization [133] and to profile the laser beam [134].

The magnetic field of permanent magnets also increases with cooling. But for the most-used Nd – Fe – B magnets, the increase in the magnetic field is replaced with its decrease at $T = 160$ K [135, 136], and at $T = 77$ K the magnetic field reverts to its room-temperature value, being dependent on the rate of cooling, unlike the field of Sm – Co magnets. At the same time, Sm – Co magnets are more expensive and have a lower magnetic energy, while the field enhancement at $T = 77$ K amounts to only 20%.

A significant change in FE characteristics under cooling permits using those materials in cryogenic FIs that are inapplicable at room temperature [129]. In particular, the authors of Ref. [137] used a gallium gadolinium garnet (GGG) with $\gamma_V \ll \gamma_p$ and demonstrated the simultaneous compensation of the depolarization and the thermal lens with FK51 glass for an FI with an AE. According to their estimate [137], the cryogenic FI with GGG can operate up to a power of 20 kW.

In Ref. [111], the FI was cooled and thermally stabilized using a Peltier element in the range 200–300 K without liquid nitrogen.

### 4.2 Magnetoactive medium selection

It is useful to introduce the figure of merit for comparing magnetooptical media. The figure of merit $V/\alpha$ was historically first introduced in Refs [123, 138, 139]. However, it characterizes only the power loss for absorption. Hereinafter, we bear in mind that the FE length $L$ is inversely proportional to $V$ for a given magnitude $B$ of the magnetic field in (1). The figures of merit $\mu$ and $\mu_{\rm i}$ were introduced more recently in [48, 140] as

$$\mu = \begin{cases} \left|\dfrac{V\kappa}{\alpha Q}\right|, & |\xi| \geqslant 1\,, \\ \left|\dfrac{V\kappa}{\alpha Q\xi}\right|, & |\xi| < 1\,, \end{cases} \qquad \mu_{\rm i} = \frac{V\kappa}{\alpha P}\,.$$

This includes all characteristics of a medium, which enter formula (12) for $p$ and formula (32) for $p_{\rm i}$: $p$ is responsible for the nondecoupling arising from the photoelastic effect and $p_{\rm i}$ for the nondecoupling caused by the isotropic thermal lens (see Table 1). In our view, it is more expedient to introduce figures of merit that have the meaning of critical power, i.e., laser power at which the parameters of a traditional FI reach certain critical values for a fixed magnetic field $B_0$. For definiteness, we assume that $B_0 = 2$ T. For the critical values, we select an isolation factor of 30 dB, i.e., $\gamma_p = \gamma_V = 0.001$, and an isotropic loss of 10% after the parabolic lens compensation, i.e., $\gamma_{\rm i,TC} = 0.1$. By equating expressions (23) and (24) to 0.001 and expression (52) to 0.1, in view of expressions (12), (25), and (32) for $p$, $p_V$, and $p_{\rm i}$, we

obtain three critical powers:

$$P_{\rm cr} = \begin{cases} \sqrt{\dfrac{0.016}{A_p}}\,\dfrac{\lambda B_0}{\pi}\left|\dfrac{V\kappa}{\alpha Q}\right|, & |\xi| \geqslant 1\,, \\ \sqrt{\dfrac{0.016}{A_p}}\,\dfrac{\lambda B_0}{\pi}\left|\dfrac{V\kappa}{\alpha Q|\xi|}\right|, & |\xi| < 1\,, \end{cases} \tag{54}$$

$$P_{{\rm cr},\,V} = \sqrt{\frac{0.064}{A_V}}\,\frac{\kappa}{\alpha}\left(\frac{1}{V}\frac{{\rm d}V}{{\rm d}T}\right)^{-1}, \quad P_{{\rm cr,i}} = \sqrt{\frac{1.6}{A_{\rm i,TC}}}\,\frac{\lambda B_0}{\pi}\left|\frac{V\kappa}{\alpha P}\right|.$$

Because all isotropic distortions are proportional to $p_{\rm i}$, $P_{\rm cr,i}$ also characterizes the medium from the standpoint of $\gamma_M$, $\gamma_S$, etc. The critical power $P_{{\rm cr},\,V}$ is responsible for the nondecoupling $\gamma_V$ caused by the $V(T)$ dependence and $P_{\rm cr}$ for all polarization distortions caused by the photoelastic effect: for the nondecoupling $\gamma_p$, as well as for the power loss $\gamma_1$ and $\gamma_{\rm a}$ during the forward passage. It is easily shown from expression (22) that the highest laser power $P_{\rm max}$ for an FI with a magnetic field of 2 T is expressed as

$$P_{\rm max} = \frac{P_{\rm cr}P_{{\rm cr},\,V}}{\sqrt{P_{\rm cr}^2 + P_{{\rm cr},\,V}^2}}\,. \tag{55}$$

As a rule, $P_{\rm cr} \ll P_{{\rm cr},\,V}$ (which is equivalent to the condition $L \gg L^*$ [see expression (26)]) and $P_{\rm max} = P_{\rm cr}$. The critical power values are given in Table 4 below. The three critical powers in (54) along with the parameter $\xi$ completely determine all thermal effects, and the higher the critical power is and the smaller $|\xi|$ are, the better the medium.

The critical powers for [111]-orientation crystals, ceramics, and glass can be obtained from formulas (54) using expressions (39)–(41). The use of crystals of other orientations requires a more sophisticated analysis [54, 141]. For $\xi > 0$, the orientation of choice is always either [111] or [001], and the choice (depending on the value of $\xi$) between these two orientations is easy to make with the help of formulas from Table 1. For $\xi < 0$, there is a polarization [119, 120, 142] denoted as [[C]] such that the eigenpolarizations are independent of the direction of mechanical stress, i.e., of transverse coordinates, and the nondecoupling completely vanishes in the absence of a magnetic field. The [[C]] orientation, which decreases the nondecoupling $\gamma_p$ significantly, albeit not to zero, has not been used in FIs but will undoubtedly be used in the future (see below). Therefore, media with $|\xi| \ll 1$ and those with $\xi < 0$ are of significant interest. Especially attractive are the respective values $\xi = -0.5$ and $\xi = -2/3$, at which $\gamma_p = 0$, for crystals of the [111] orientation and ceramics [see expressions (39) and (40)].

At present, TGG crystals are used in the majority of FIs for a wavelength of 1 μm. This is attributable to their high thermal conductivity in comparison with glasses, on the one hand, and, on the other, to the high Verdet constant $V$, wide aperture, and high manufacturability in comparison with those of other crystals (see Table 4). The search for new media for FIs is traditionally aimed at increasing $V$. Crystals and ceramics have been obtained whose $V$ exceeds that of TGG by several tens of percent: TAG [143, 144], TSAG [145–147], TSALG [148–150], doped TAG ceramics [71,151,152], doped TGG crystals [153–156], $TbVO_4$ [157], $Tb_2Sn_2O_7$ [158], $Dy_2Ti_2O_7$ [159], $CaTbAlO_4$ [160], $Sr_2Tb_8(SiO_4)_6O_2$ [161], $Li_2Tb_4(MoO_4)_7$ [162], $Na_2Tb_4(MoO_4)_7$ [163], $NaTb(WO_4)_2$ [164], etc. The record holders are the $Tb_2O_3$ crystal [165] and ceramics [166], whose $V$ is 3.5 times greater than for TGG. Further advancement in this direction is possible, but attempts to significantly increase $V$ will hardly meet with success. At the same time, $P_{\rm cr}$ depends on other parameters ($\alpha$, $\kappa$, $Q$, and $\xi$) no less than on $V$. Therefore, to radically increase $P_{\rm cr}$, the quest for media should be pursued along three lines.

The first are media with $V$ values comparable with or lower than those in TGG. In this case, a significant decrease in $\alpha$ or increase in $\kappa$ would hardly be expected, a radical decrease in $Q$ and (or) the 'residence' of $\xi$ within the desired domain are possible: $|\xi| \ll 1$ and $\xi < 0$. There are inspiring examples of this kind already: TSAG crystals with a very low $Q$ and $Na_{0.37}Tb_{0.63}F_{2.26}$ (NTF) crystals with $\xi = -0.37$ (see Table 4). For a TSAG crystal, the condition $P_{\rm cr} \ll P_V$ is violated even at room temperature and $P_{\rm max} = P_V$. However, TSAG has a significant drawback: the large modulus of $\xi$ ($\xi = -101$ [167]). In this case, the terms of the order of $p^4$, in particular $p^4\xi^4$, cannot be ignored in expression (23) for $\gamma_p$. The inclusion of this term leads to a decrease in $P_{\rm cr}$ and hence in $P_{\rm max}$ by more than a factor of ten. Furthermore, the forward-passage power loss $\gamma_1$ (see Table 1) is proportional to $\xi^2$. Requiring that the inequality $\gamma_1 < 0.1$ be satisfied, we obtain $P_{\rm max} = 0.1P_{\rm cr}$. In view of expressions (39) and (40), for such a large $\xi$ modulus, it is also 'inexpedient' to use crystals of the [111] orientation and ceramics, as well as FIs with the depolarization compensation described in Section 3. The negative sign of $\xi$ in TSAG crystals offers no significant advantages: for such a large $|\xi|$, the [[C]] orientation is close to [001] [167]. Another example is the NTF crystal [121]: for the $V\kappa$ product six times lower than for TGG, it offers a much higher critical power $P_{\rm cr}$ (see Table 4). Furthermore, its negative $\xi$ permits an efficient use of the [[C]] orientation, which is [[76 65 76]] for $\xi = -0.37$ (see Ref. [168]). All the above circumstances contribute to the lowering of $\gamma_p$ without changing $\gamma_V$.

Second, of interest are the media that contain little or no terbium at all. The $V$ values in such media will supposedly rank well below those in TGG. However, in this case it is reasonable to expect a significant decrease in $\alpha$ or increase in $\kappa$, as well as, as in the former case, a decrease in $Q$ and (or) the residence of $\xi$ in the desired domain. Then the region of search becomes substantially broader. An example is provided by $CaF_2$ crystals doped with 10 atomic percent of terbium: $Tb{:}CaF_2$ [169]. This crystal ranks below TGG in $V$ (tenfold) and in $\kappa$ (twofold), but the improvement in $\alpha$, $Q$, and $\xi$ compensates this with a safety margin: in a 29 mm long crystal, the depolarization remained 'cold' up to a power of 1.5 kW [169]. This gives a lower estimate of the critical power: $P_{\rm cr} = 5$ kW, which is much higher than for TGG (see Table 4). The $\xi$ value for $Tb{:}CaF_2$ is unknown, but in undoped $CaF_2$, $\xi = -0.47$ [120] and the [[C]] orientation is close to [111]. We note that low $V$ values result in an increase in $L$, which complicates the design of the magnetic system. At the same time, $\gamma_V$ can be disregarded in this case [see expressions (20) and (26)].

Third, a small but simultaneous improvement in some or even all parameters ($V$, $\alpha$, $\kappa$, $Q$, and $\xi$) is of course possible, resulting in a significant cumulative increase in $P_{\rm cr}$.

All results obtained above pertain to cubic crystals of m3m symmetry. Cubic crystals and ceramics of lower symmetry m3, for instance, the sesquioxide $Tb_2O_3$ or $Nd{:}La{:}Y_2O_3$ [170] mentioned above, require a more sophisticated analysis of thermally induced effects, which was

performed in Refs [142, 171, 172]. For anisotropic crystals, for instance, $TbAlO_3$ [173], the problem is even more intricate [174].

However, glasses should not be completely disregarded, despite their lower thermal conductivity than that of crystals. For all glasses, $\xi = 1$; as regards $Q$, its magnitude can be efficiently controlled by varying the composition. For instance, among laser glasses, there is quartz neodymium glass with $Q = 0.2 \times 10^{-7}\ \mathrm{K}^{-1}$ [175, 176], which is nearly two orders of magnitude lower than in TGG. If a magnetoactive glass with this $Q$ were made, its critical power $P_{\mathrm{cr}}$ would be higher than for TGG. The recent development of borogermanate glass TBG with a content of terbium oxide [177, 178], not all of whose parameters have been measured (see Table 4), may be the first step on this path.

To measure the critical powers $P_{\mathrm{cr}}$ and $P_{\mathrm{cr,i}}$, it is useful to measure the dependences of $\gamma_p$ and $F$ on the radiation power $P_0$. Table 4 gives the values of $P_{\mathrm{cr}}$ and $P_{\mathrm{cr,i}}$ calculated from the experimental data of the corresponding papers with the use of expressions (23) and (25). Quite frequently, absorption varies from sample to sample, which may lead to variations in the values of $\alpha$ itself, as well as of $P_{\mathrm{cr}}$ and $P_{\mathrm{cr,i}}$. Without going into the details, we only mention some papers devoted to the measurements of $V$ [121], $\alpha$ [179, 180], $\kappa$ [181–183], $Q$ [50, 54, 117, 167], $P$ [109, 117, 167], $\xi$ [54, 117], and the sign of $\xi$ [120].

At present, apart from TGG crystals, TSAG and TSLAG crystals as well as TGG and TFG ceramics are used in FIs (see Table 3).

### 4.3 Enhancement of the magnetic field

An increase in the magnetic field $B$ results in a proportional shortening of the FE [see expression (1)] and an increase in the maximum radiation power $P_{\max}$. An FI with a superconducting solenoid with $B = 5$ T was described in Ref. [136]. Attaining such (and even higher) fields at room temperature is possible only in a pulsed mode, which hinders the use of FIs in lasers with a high pulse repetition rate and fully rules out the application of FIs in cw lasers. This is the reason why permanent magnets are actually used in nearly all cases.

Wide acceptance has been gained by magnetic systems consisting of radially and axially magnetized rings [105, 184–187], which produce a magnetic field $B \approx 1$ T. As shown in Ref. [64], it is very difficult to attain a magnetic field value above 1.5 T in such systems, and hence the use of magnetic circuits was proposed, with the result that a field $B = 2.1$ T was obtained.

Attempts to further enhance the field by increasing the dimensions of the magnetic system quickly result in an unreasonable increase in its mass. This is due to the logarithmic dependence of the maximum attainable field on the ratio of the outer and inner magnet diameters [187]. The use of ferromagnetic alloys with a strong residual induction does not lead to the desired field increase due to the sequential degaussing of a part of the central ring. To solve this problem, the authors of Ref. [188] calculated the field in the entire volume of the magnetic system, including the portions filled with magnets, and revealed the domains most prone to

**Table 3.** Faraday isolators.

| FI | Diameter $D$, mm | Length $L$, mm | FE material* | $\alpha$, $10^{-3}\ \mathrm{cm}^{-1}$ | $P_0$, W | $I = -10\lg\gamma$, dB | $P_{\max}$, W | Reference | Year |
|---|---|---|---|---|---|---|---|---|---|
| Traditional FI | | 120 | MOG04** | | 400 | 7 | 25 | [49] | 2000 |
| | | 30 | MOG04 | | 260 | 23 | 100 | [61] | 2015 |
| | 10 | 20 | TGG [001] | 3 | 77 | 33 | 125 | [52] | 2000 |
| | 8 | 25 | TGG | — | 550 | 15 | 100 | [62] | 2006 |
| | 5.5 | 16 | TGG | | 200 | 22 | 100 | [73] | 2010 |
| | 20 | 28 | TGG [001] | 3 | 750 | 13.5 | 110 | [63] | 2007 |
| | 20 | 18 | TGG [001] | 2.5 | 176 | 30 | 176 | [63] | 2007 |
| | 13 | 10.3 | TGG [001] | 2.5 | 330 | 31 | 400 | [64] | 2009 |
| | 20 | 18 | TGG [001] | 2 | 330 | 20 | 113 | [65] | 2011 |
| | 20 | 18 | TGG [001] | 2 | 330 | 25.5 | 200 | [66] | 2012 |
| | 13 | 10.5 | TGG [001] | 2.3 | 330 | 32.6 | 450 | [66] | 2012 |
| | 10 | 20 | TGG [111] | 1.9 | 260 | 22.8 | 115 | [66] | 2012 |
| | 13 | 9 | TGG [001] | 1.3 | 650 | 30 | 650 | [67] | 2013 |
| | 13 | 9 | TGG [001] | 1.3 | 800 | 29 | 650 | [68] | 2014 |
| | 7 | 9.2 | TGG ceramics | 1.4 | 260 | 33 | 340 | [69] | 2014 |
| | 7 | 7 | TAG ceramics | | 300 | 38 | 700 | [70] | 2014 |
| | 13 | 8 | Ce:TAG ceramics | | 300 | 31 | 330 | [71] | 2014 |
| | 6 | 7 | TSAG [111] | 2.5 | 500 | 32 | 600 | [72] | 2014 |
| | | | TSAG [001] | | 1500 | 35 | > 1500 | [74] | 2015 |
| | 3 | 10 | TSLAG | | | 48 | | [148] | 2013 |
| $\lambda/2$ FI | | 120 | MOG04** | | 400 | 16 | 200 | [49] | 2000 |

**Table 3** (continued).

| FI | Diameter $D$, mm | Length $L$, mm | FE material* | $\alpha$, $10^{-3}$ cm$^{-1}$ | $P_0$, W | $I = -10 \lg \gamma$, dB | $P_{max}$, W | Reference | Year |
|---|---|---|---|---|---|---|---|---|---|
| FI with RR | | 120 | MOG04** | | 400 | 25 | 250 | [49] | 2000 |
| | 10 | 22 | TGG [001] | 3 | 73 | 45 | 450 | [52] | 2000 |
| | 4 × 8 | 15 | TGG | — | 1180 | 14.7 | — | [62] | 2006 |
| | 20 | 28 | TGG [001] | 3 | 750 | 24 | 600 | [63] | 2007 |
| | 20 | 18 | TGG [001] | 2.5 | 180 | 42.6 | — | [63] | 2007 |
| | 30 | 21.4 | TGG [001] | 1.5 | 1500 | 30 | 1500 | [68] | 2014 |
| | 30 | 21.4 | TGG [001] | 1.5 | 1500 | 33*** | > 2500 | [68] | 2014 |
| | 40 | 27.2 | TGG [001] | 1.3 | 700 | 34 | ~ 1900 | [106] | 2015 |
| | 20 | 19 | TGG [001] | | 250 | 38 | 600 | [107] | 2012 |
| | 20 | 19 | TGG [001] | | 100 | 49 | > 1000 | [107] | 2012 |
| | 7 | 14 | TGG ceramics | 1.4 | 740 | 35 | 1500 | [108] | 2014 |
| | 13 | 8 | Ce:TAG ceramics | | 300 | 39 | > 1000 | [71] | 2014 |
| | 6.3 | 10.4 | TSAG [111] | 2.5 | 350 | 32 | 400 | [109] | 2015 |
| FI with AE | 20 | 18 | TGG [001] + TGG [001] | 2 | 330 | 35.7 | 600 | [65] | 2011 |
| | 20 | 18 | TGG [001] + $CaF_2$ [001] | 2 | 330 | 31 | 430 | [66] | 2012 |
| | 13 | 10.5 | TGG [001] + $CaF_2$ [001] | 2.3 | 330 | 38.9 | 880 | [66] | 2012 |
| | 13 | 9 | TGG [001] + $CaF_2$ [001] | 1.3 | 1100 | 30 | 1100 | [68] | 2014 |
| | 10 | 20 | TGG [111] + $CaF_2$ [001] | 1.9 | 260 | 27 | 200 | [66] | 2012 |
| | 7 | 9.2 | TGG ceramics + TGG ceramics | 1.4 | 300 | 38 | 900 | [110] | 2014 |
| | 7 | 9.2 | TGG ceramics + TGG [001] | 1.4 | 300 | 37 | 750 | [110] | 2014 |

* MOG04 — a sort of magnetoactive optical glass, TGG — terbium–gallium garnet, TSAG — terbium–scandium–aluminum garnet, TSLAG — terbium–scandium–lutetium–aluminum garnet.
** Experiment was performed at $\lambda = 532$ nm; indicated are the equivalent-power values for $\lambda = 1064$ nm and the FE length $L = 40$ mm.
*** Angle of rotation of the reciprocal rotator is 73°.

degaussing. The magnets were removed from these domains, which resulted in an increase in $B$ to 2.5 T (despite a smaller number of magnets). Adding more magnetic circuits lowered the aperture from 13 mm to 7 mm but increased the field to $B = 2.87$ T [168].

Also of interest is the use of rings magnetized not only radially and axially but also angularly. This complicates the structure but permits enhancing the magnetic field [189]. A magnetic system of parallelepiped-shaped magnets was described in Ref. [190].

### 4.4 Disc and rectangular geometries of heat removal

In Sections 2 and 3, we considered the so-called rod-shaped geometry (see Fig. 2), i.e., we assumed that the FE is cooled only in the radial direction ($\mathrm{d}T/\mathrm{d}z = 0$). This cooling is used nearly always, because it is practically convenient. Less convenient is longitudinal heat removal in the disc geometry (Fig. 12a). It permits diminishing the thermal effects in an FI by weakening transverse temperature gradients (longitudinal gradients do not give rise to thermal distortions). To remove heat, a gas flow or the diffusion bonding of a TGG crystal, for instance, to YAG, sapphire, or diamond can be used. In Ref. [191], analytic expressions were derived for $\gamma_p$ and $\gamma_V$ for a traditional FI, a $\lambda/2$ FI, and an FI with RR under a thin-disc approximation ($h/r_0 \ll 1$, where $h$ is the disc thickness). It was shown that as in the rod-shaped geometry, the nondecoupling is determined by the photoelastic effect, i.e., $\gamma_p \gg \gamma_V$. The depolarization in the traditional FI is proportional to $(h/r_0)^4$, which was experimentally observed in Ref. [192], while in $\lambda/2$ FIs and FIs with RR, it is proportional to $(h/r_0)^8$. To decrease $h/r_0$, several discs can be used. The disc geometry offers significant advantages even when $h/r_0$ is of the order of unity. A reduction in depolarization was experimentally observed in the disc geometry in a cryogenic FI [128]. At room temperature, phase distortions decreased twofold for $h = 1.6r_0$ in Ref. [131], in perfect agreement with numerical simulation data. We note that the thermooptical constant $Q$ in the disc geometry is somewhat different from the one in (8): $Q_{\mathrm{disc}} = Q(1 - \nu)$ [20].

Another approach consists in passing to a rectangular geometry: an FE in the form of thin plates (Fig. 12b). In this case, the laser beam must also be rectangular or elliptical in shape. As in the rod-shaped geometry, cooling is effected in the transverse direction. The decrease in nondecoupling in this case is attributable to the fact that the direction of the temperature gradient is the same throughout the cross section. In the thin-plate approximation ($t \ll w$, where $t$ is the thickness and $w$ is the width), the problem was solved analytically [89] for a traditional FI, a $\lambda/2$ FI, and an FI with RR. It was shown that the nondecoupling is determined by the photoelastic effect, i.e., $\gamma_p \gg \gamma_V$. The non-

**Table 4.** Properties of magnetoactive media.*

| Parameter / Material | $V$, rad T$^{-1}$ m$^{-1}$ | $V^{-1}\,\mathrm{d}V/\mathrm{d}T$, $10^{-3}$ K$^{-1}$ | $\kappa$, W K$^{-1}$ m$^{-1}$ | $\alpha$, $10^{-3}$ cm$^{-1}$ | $\xi$ | $\alpha_T$, $10^{-7}$ K$^{-1}$ | $Q$, $10^{-7}$ K$^{-1}$ | $\mathrm{d}n/\mathrm{d}T$, $10^{-6}$ K$^{-1}$ | $P$, $10^{-6}$ K$^{-1}$ | $P_{\mathrm{cr}}$, kW | $P_{\mathrm{cr},V}$, kW | $P_{\mathrm{cr,i}}$, kW |
|---|---|---|---|---|---|---|---|---|---|---|---|---|
| TGG | 39 [194, 195]<br>35 [196–198]<br>36 [127]<br>40 [199]<br>37 [109] | 3.5 [125]<br>≈ 3.4 **** | 4.4 ± 0.1 [200]<br>4.5 ± 0.5 [130]<br>5.3 ± 0.5 [201]<br>4.2 ± 0.3 [181] | 2 [116]<br>2.5 [64]<br>1.6 [114]<br>1.3 [128]<br>4.9 [202] (cer.) | 2.2 [54]<br>2.25 [117] | 94 [116]<br>67–72 [200]<br>40 [198]<br>73 [203] | −17 ** [117]<br>−15 *** [117] | 20 [116]<br>19 [117]<br>18–21 [200]<br>18 [203] | 17 ** [117] | 0.65 | 21 | 1.2 |
| TGG, 80 K | ≈ 132 [127] | ≈ 12.5 **** [126] | 5, from melt<br>10, from flux [130] | 2.6 [128] | 1.3 [129] | 12 [203] (86 K) | −3 ** [128] | 6 [203] (86 K) | 2.5 [128] | 6.1 | 3 | 14 |
| TSAG | 46.0±0.3 [109]<br>= 1.2$V_{\mathrm{TGG}}$ [145]<br>= 1.2$V_{\mathrm{TGG}}$ [148, 149] (TSLAG) | ≈ 3.4 [204] | 3.6 ± 0.3 [167] | 2.5 [109]<br>≈ $\alpha_{\mathrm{TGG}}$ [148, 149] (TSLAG) | −101 ± 10 [167] | 62 [150]<br>64 [150] (TSLAG) | −0.4 ****** | | = 800$Q$ [167]<br>= 1300$Q$ [109] | 22 [167]<br>2.2 *****<br>0.17 ([111] orientation) [109]<br>0.4 ([111] orientation) [72] | 3.9 | 0.49 [167]<br>0.15 ([111] orientation) [109] |
| $Na_{0.37}Tb_{0.63}F_{2.26}$ (NTF) | ≈ 30.5 [121] | | 1 [168] | | −0.37 [168] | | | | | > 1.3 [168] | | |
| TAG ceramics | 51 [143] (mono)<br>45 [70] | | 6.5 [144]<br>5.00±0.35 [181] | | | | | | = 19$Q$ [70] | 0.67 [70]<br>0.58 [205] | | 0.65 [70] |
| CeTaG ceramics | 53 [71]<br>(0.1 at.% Ce) | | 5.00±0.35 [181] | | | | | | = 18$Q$ [71] | 0.38 [71] | | 0.34 [71] |
| Tb:$CaF_2$ | 4 [169] | ≈ 3.4 [169] | 2.2 [169] | | −0.47 [120] ($CaF_2$) | | | | | > 5 [169] | | |
| TBG | 32 [177]<br>35 [178] | ≈ 3.4 [178] | 0.8 ± 0.1 [178] | 1 [177]<br>≈ 20 [178] | 1 | 75 [177] | | | = 17$Q$ [178] | 0.014 [178] | 4.2 | 0.005 [178] |
| MOG105 | 17 [194]<br>18 [195, 206] | 5 [206] | 0.51 [50] | 2.3 [206] | 1 | 82 [207] | 6 [50] | 0.6 [207] | | 0.046 | 0.86 | |
| MOG04 | 21 [194, 195, 206] | ≈ 3.4 **** | 0.74 [50] | 1 [194]<br>2.3 [206] | 1 | 49 [207] | 9 [50] | 8.7 [207] | | 0.125<br>0.06 [178] | 3.9 | |
| MOG10 | 28 [195, 206]<br>26 [194] | ≈ 3.4 **** | 0.68 [50] | 2 [194]<br>4.6 [206] | 1 | 56 [207] | 8.5 [50] | 8.5 [207] | | 0.078 | 1.8 | |
| FR-5 | 21 [194, 197] | 3.4 [208] | 0.84 [116] | 3 [194] | 1 | 47 [116] | 9 [50] | 7.5 [116] | | 0.047 | 1.6 | |

* $P_{\mathrm{cr}}$, $P_{\mathrm{cr},V}$, and $P_{\mathrm{cr,i}}$ values were calculated from the experimental data of the corresponding studies with the use of formula (54) (the values without source references were calculated by formula (54) proceeding from the best values given in the table). The $Q$ values for glasses are given in magnitude.

** It is assumed that $\kappa = 5$ W K$^{-1}$ m$^{-1}$.

*** It is assumed that $\kappa = 4.4$ W K$^{-1}$ m$^{-1}$.

**** It is assumed that $V$ is proportional to $1/T$.

***** Recalculation in view of the high $\xi$ value.

****** Obtained by processing the data in Refs [109, 167].

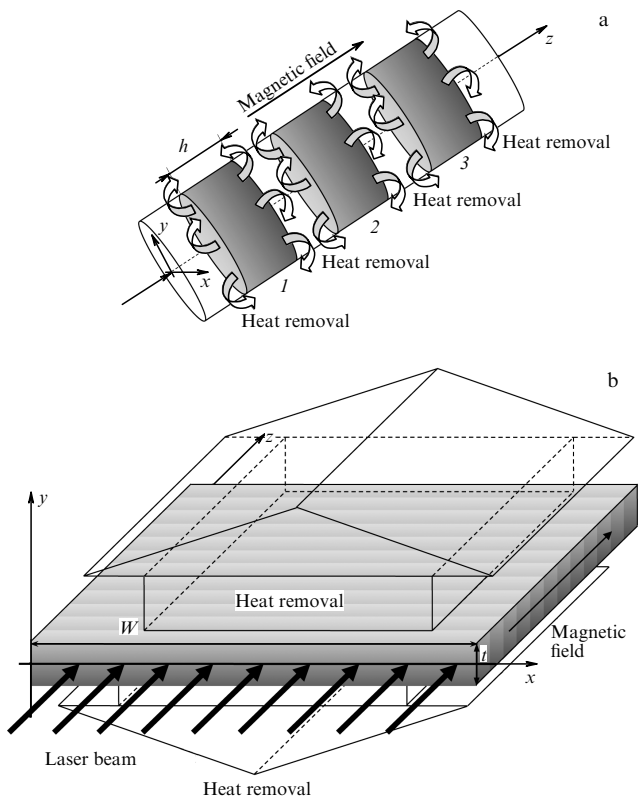


**Figure 12.** (a) Disc and (b) rectangular geometries of the magnetoactive element.

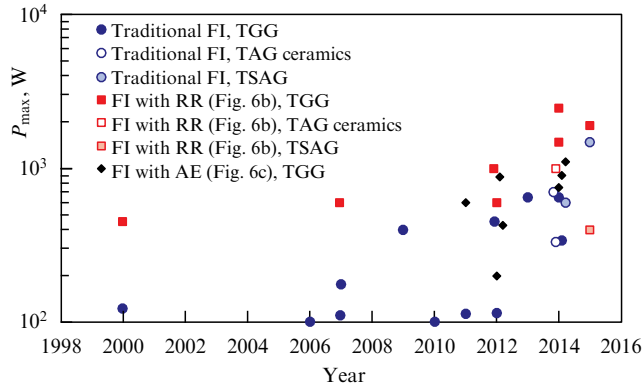


**Figure 13.** Maximum FI power $P_{max}$ (the power at which the isolation ratio is equal to 30 dB).

decoupling in traditional FIs is proportional to $(t/w)^2$, while in $\lambda/2$ FIs and FIs with RR it is proportional to $(t/w)^4$. Therefore, the rectangular geometry provides the greatest gain for beams with a high aspect ratio, $w/t \gg 1$. Furthermore, in FIs for depolarized radiation, the rectangular geometry of the FE permits two circular beams to be optimally arranged in the FE aperture, which also increases the FI isolation ratio [61].

Special features of the thermooptics of square-aperture FIs were investigated in Ref. [193].

## 5. Conclusions

We briefly list the results outlined in this paper and discuss avenues of further research.

### 5.1 Results

We summarize the results described above (see also Figs 13 and 14).

(1) The absorption of radiation in a magnetoactive medium results in a transversely nonuniform temperature distribution, which gives rise to three mechanisms of the action on laser radiation: depolarization due to the photoelastic effect, depolarization due to the temperature dependence of the Verdet constant $V(T)$, and a thermal lens. These three effects are completely determined by three parameters: $p$ in (12), $p_V$ in (25), and $p_i$ in (32), which have the meaning of the dimensionless power of laser radiation, as well as by the optical anisotropy parameter $\xi$ in (9); the smaller $|\xi|$ is, the better.

(2) Thermally induced distortions in FIs are characterized by the following parameters:

— first and foremost, by the nondecoupling $\gamma$ — the inverse FI isolation ratio (3). The nondecoupling $\gamma$ consists of two terms, $\gamma_p$ and $\gamma_V$, due to the photoelastic effect and the $V(T)$ dependence;

— second, by the thermally induced polarization power loss $\gamma_1$ in the forward passage through an FI;

— third, by the amplitude and phase beam distortions in the forward passage, which consist of the anisotropic loss $\gamma_a$ arising from the photoelastic effect, and the isotropic loss due to the temperature dependence of the refractive index and the isotropic part of the photoelastic effect. Isotropic distortions are conveniently characterized by either a decrease in $\gamma_i$ given by (31) in the overlap integral or by a decrease in the Strehl number $\gamma_S$ or an increase in the parameter $M^2$, which is determined by the quantity $\gamma_M$ in (34). The expressions for all $\gamma$ are collected in Table 1.

(3) The parameters $p$, $p_V$, and $p_i$ are determined by the wavelength $\lambda$, by the length $L$ of the Faraday element, which is inversely proportional to $V$ in (1) for a given magnetic field $B$, and by the characteristics of the magnetoactive medium. Therefore, for given $B$ and $\lambda$, the thermal effects are determined only by the material constants of the medium. Consequently, to compare different media and to compare different thermal effects, it is expedient to introduce three critical powers: $P_{cr}$, $P_{cr,V}$, and $P_{cr,i}$, Eqn (54), which are the powers of laser radiation at which the parameters of a traditional FI reach certain critical values: specifically, an isolation ratio of 30 dB, i.e., $\gamma_p = \gamma_V = 0.001$, and an isotropic loss of 10% after compensation of the parabolic phase, i.e., $\gamma_{i,TC} = 0.1$. The higher the critical power is, the better the medium. The highest laser power $P_{max}$ at which the FI ensures an isolation $> 30$ dB is determined from expression (55). For $B = 2$ T and $\lambda = 1.06$ μm, the values of $P_{cr}$, $P_{cr,V}$, and $P_{cr,i}$ are given in Table 4, whence it is seen that, typically, $P_{cr} \ll P_{cr,V}$. This signifies that $\gamma_V \ll \gamma_p$, and the temperature dependence of the Verdet constant can be neglected. In this case, $P_{max} = P_{cr}$. Exceptions are provided by cryogenic FIs and TSAG crystals of the [001] orientation.

(4) New FIs permit compensating the depolarization caused by the photoelastic effect, i.e., significantly decreasing the nondecoupling $\gamma_p$: an FI with a $\lambda/2$ plate (Fig. 6a), an FI with a reciprocal polarization rotator (Fig. 6b), and an FI with an absorbing optical element (Fig. 6c). The nondecoupling in these FIs, as in traditional FIs (see Fig. 1), is determined by only two parameters, $p$ and $\xi$; but unlike $\gamma_p$ in traditional FIs, $\gamma_p$ in these FIs is proportional not to $p^2$

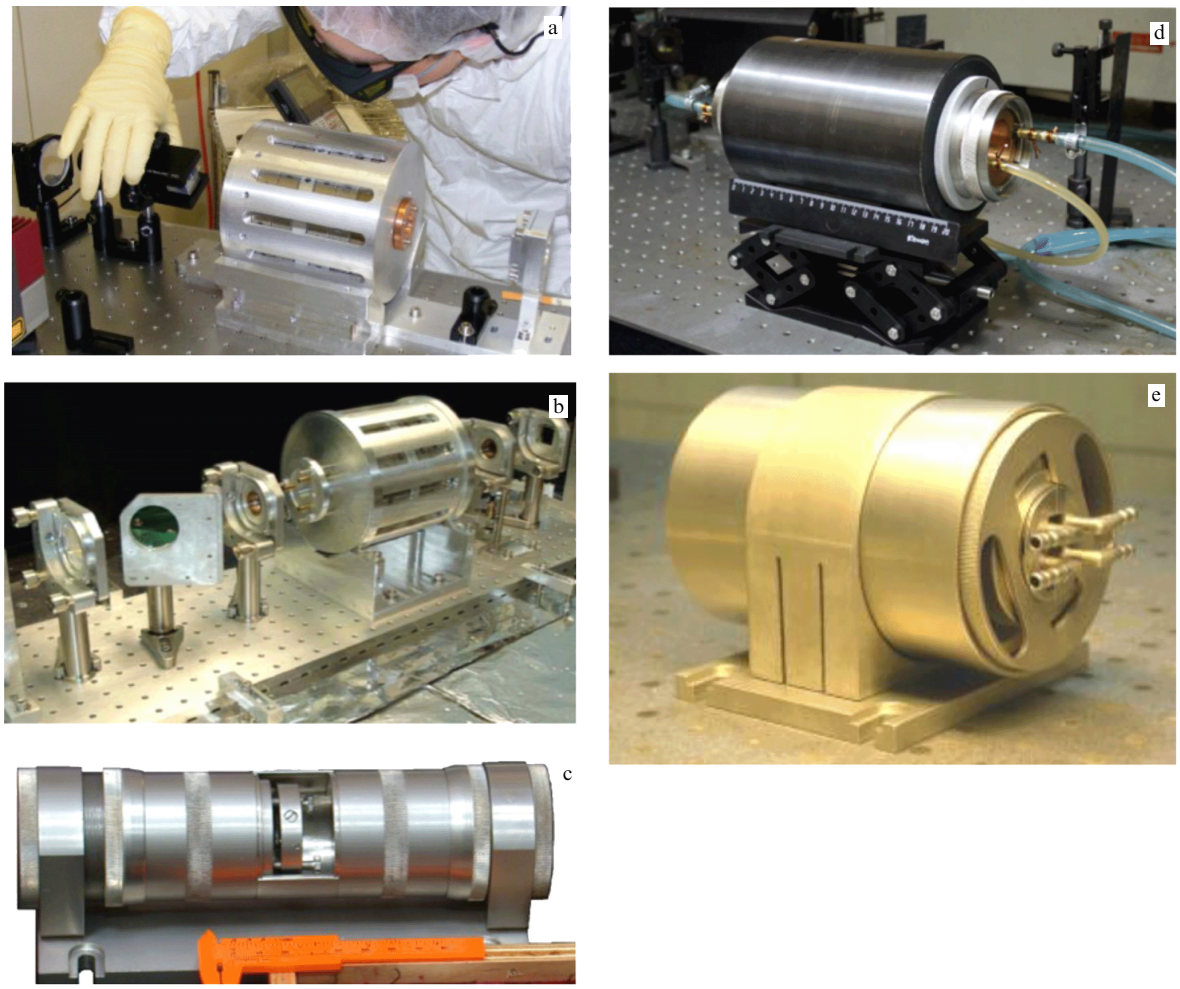


**Figure 14.** Faraday isolators for the (a) LIGO, (b) Virgo, and (c) GEO gravitational wave detectors, as well as isolators (d) with an aperture of diameter 40 mm and (e) with a rectangular aperture.

but to $p^4$ [see expression (46)]. The minimal nondecoupling is provided by FIs with a reciprocal rotator (see Fig. 7); however, the other two types of FIs offer advantages of their own. New FIs have been investigated in many studies for a laser power up to 1.5 kW (see Table 3 and Figs 8 and 9). For a low power, the nondecoupling is defined by 'cold' depolarization, but as the power increases, it also increases and tends to the theoretical values of $\gamma_p$ in (46), shown by solid lines in Figs 8 and 9.

(5) Isotropic phase distortions can be compensated (see Fig. 5) in two ways: with a parabolic lens (telescope compensation) or with an absorber with a thermal lens of the opposite sign (adaptive compensation). Because the thermal lens is nonparabolic, the telescope method by no means provides complete compensation of the isotropic distortions $\gamma_{\rm i}$ and $\gamma_S$, but does not decrease $\gamma_M$ at all, because the parameter $M^2$ is independent of the parabolic phase. At the same time, the telescope method does not result in an additional increase in the losses $\gamma_{\rm l}$ and $\gamma_{\rm a}$. Adaptive compensation, on the contrary, ensures zero isotropic distortions $\gamma_{\rm i}$, $\gamma_S$, and $\gamma_M$, but increases the losses $\gamma_{\rm l}$ and $\gamma_{\rm a}$ due to the photoelastic effect in the absorber (see Table 1). To eliminate this drawback, an anisotropic crystal should be used as the absorber, for instance, DKDP or a crystal with negative $\xi$ of the [[C]] orientation, say, $CaF_2$. In this case, $\gamma_{\rm i} = \gamma_S = \gamma_M = 0$, with no increase in either $\gamma_{\rm l}$ or $\gamma_{\rm a}$, as in the telescope method.

(6) All thermally induced effects, with the exception of the temperature dependence of the Verdet constant, can be significantly diminished in a cryogenic FI. On cooling a TGG crystal to $T = 77$ K, the parameters $p$ and $p_{\rm i}$ decrease [see Eqn (53)] and the critical powers $P_{\rm cr}$ and $P_{\rm cr,\,i}$ increase by about a factor of ten. A decrease in $\xi$ also diminishes distortions (see Table 1). But $p_V$, on the contrary, increases approximately 7.2-fold, and therefore $P_{{\rm cr},\,V}$ decreases by a factor of 7.2, to become smaller than $P_{\rm cr}$. As a result, the $V(T)$ dependence contributes to the nondecoupling even more than the photoelastic effect, and the maximum power $P_{\rm max} \neq P_{\rm cr}$ is defined by expression (55).

(7) At present, in the overwhelming majority of cases, the TGG crystals are used in FIs for a wavelength of 1 μm, which is due to the higher thermal conductivity than in glasses, as well as the large Verdet constant $V$, wide aperture, and a high manufacturability of TGG crystals in comparison with other crystals. However, recent years have seen a variety of alternative crystals and ceramics, and some of them have or may have better characteristics: higher values of critical powers $P_{\rm cr}$, $P_{{\rm cr},\,V}$, and $P_{\rm cr,\,i}$. Data about some of the most promising of them are collected in Table 4: TSAG, NTF, TAG ceramics, Tb:$CaF_2$.

(8) All formulas given in this paper apply to a Gaussian beam and a crystal of the [001] orientation. They can be easily generalized to crystals of the [111] orientation, ceramics, and glass by formal change (39), (40), and (41), as well as to a super-Gaussian beam, for which only the numerical coefficients $A$ given in Table 2 are changed. We note that all distortions, without exception, are independent of the beam diameter.

(9) An increase not only in the critical power $P_{cr}$, which is determined by the magnetoactive medium, but also in the magnetic field $B$ leads to a decrease in the nondecoupling. Over the past ten years, the magnetic field in FIs has been increased approximately twofold: from 1–1.5 T to a present record value of 2.5–2.86 T. This has permitted shortening the Faraday elements by about a factor of two and, accordingly, increasing the maximum radiation power.

### 5.2 Further research

In our view, research into the FIs for 1 μm lasers with a high average power will be pursued most vigorously along the following lines.

The *quest for alternatives to TGG crystals* has been actively pursued in recent years and will be continued. Of greater significance are higher values of the critical powers $P_{cr}$, $P_{cr,V}$, and $P_{cr,i}$ in (54), rather than higher values of the Verdet constant and the optical anisotropy parameter $\xi$ in (9). Of interest are media with $|\xi| \ll 1$, because the nondecoupling for $|\xi| < 1$ is proportional to $\xi^2$, and media with $\xi < 0$ for which the [[C]] orientation exists, which permits a significant reduction in the nondecoupling. Especially compelling are the respective values $\xi = -0.5$ and $\xi = -2/3$, at which the birefringence vanishes completely in [111]-orientation crystals and in ceramics. Ceramic elements can be fabricated of materials that are extremely hard to grow in the form of single crystals, and this significantly broadens the area of the search for new media. In particular, the $Tb_2O_3$ ceramics has made its appearance, which has an m3 symmetry (lower than in garnets and fluorides), like all sesquioxides. This complicates analyzing thermally induced effects but at the same time yields an additional degree of freedom for their compensation. Also of interest is the use of anisotropic crystals in FIs. Determining $P_{cr}$, $P_{cr,V}$, $P_{cr,i}$, and $\xi$ for the new materials requires high-quality samples (desirably, of the [001] orientation) and accurate measurements.

An important feature of *TSAG crystals is the large value* $|\xi| = 101$, which introduces qualitative differences into FIs with this crystal, which is one of the most promising alternatives to the TGG crystal. As discussed in the foregoing, the quantity $\gamma_p = A_p p^2$ in Eqn (23) no longer determines the nondecoupling because the next term (to be denoted as $\gamma_\xi$), proportional to $p^4\xi^4$, becomes more significant. For $|\xi| = 101$, the critical power amounts to 0.078 of the $P_{cr}$ value defined by formula (55). This signifies that precisely $\gamma_\xi$ must be lowered in order to achieve compensation, and there is no need to diminish $\gamma_p$, which is the objective of the FIs depicted in Fig. 6. The strategy to solve this problem has not yet been proposed. Furthermore, in TSAG, the polarization loss $\gamma_1$ in the forward passage also limits the radiation power to a greater degree than the nondecoupling does: $\gamma_1 = \xi^2\gamma_p = 10{,}000\gamma_p$. Requiring the inequality $\gamma_1 < 0.1$ to be satisfied, we obtain $P_{max} = 0.1P_{cr}$. Consequently, it is $\gamma_1$ that should be diminished and not $\gamma_p$, as usual; but the nondecoupling $\gamma_p$ must not increase, so as not to throw the baby out with the bath water. To this end, it is possible to propose, for instance, the use of an FI with a reciprocal rotator (Fig. 6b) and an FI with an absorber (Fig. 6c) if the forward and backward passes change places; in this case, $\gamma_p$ and $\gamma_1$ also change places. As a result, the nondecoupling becomes independent of $\xi$ and the power loss in the first passage (although proportional to $p^4\xi^4$) is under 10% for a power up to the $P_{cr}$ value defined by formula (55). To state it in different terms, for such a large $\xi$ value, it is required that the dependence of depolarization in both passes (and not only in the backward one, as is usually the case) on $\xi$ (and not on the power, as is usually the case) diminish. Of interest is the study of the dependence of $\xi$ and $Q$ on the scandium content in TSAG, as well as the measurement of these parameters in TSLAG and TAG crystals.

*To decrease the nondecoupling $\gamma_V$, it is possible* to use an additional short FE embedded in a magnetic field of the opposite sign. Owing to its short length, this second FE would rotate the polarization through a small angle (for instance, $-5°$), which is easy to compensate by increasing the rotation angle of the principal FE from 45° to 50°. If the second FE has a higher absorption or a lower thermal conductivity (for instance, by 10 times), then as the power increases, the variation of the rotation angle in the two FEs is equal in magnitude and opposite in sign. This is actually equivalent to an FE with the reversed sign of $dV/dT$. By selecting the parameters of the second FE (length, orientation, direction of crystallographic axes, and the material), it is possible to optimize $\gamma_1$ and $\gamma_p$ simultaneously with decreasing $\gamma_V$. This adaptive approach, whereby distortions accumulate in one element and are subtracted in the other (as in the methods for compensating the depolarization and the thermal lens described in Section 3), seems to show greater promise than magnetic field profiling, efficient only for a specific power value.

To date, the *longitudinal nonuniformity of the magnetic field* has not been used to diminish depolarization. At the same time, high magnetic fields with strong longitudinal gradients are now available. This determines the importance of the optimization problem of the longitudinal field distribution for compensating the thermally induced depolarization. We note that the magnetic field can be alternating in sign, which substantially broadens the potentialities of the search for optimal distributions.

The *disc and rectangular geometries of heat removal* show great promise from the theoretical standpoint but have been studied insufficiently. The progress of diffusion disc bonding technology and magnetic field optimization for the rectangular geometry, especially for a high aspect ratio, will permit developing these little-used techniques for lasers with a high average power in the future.

**Acknowledgements**. The author expresses his deep gratitude to his colleagues O V Palashov, I V Mukhin, D S Zheleznov, I L Snetkov, E A Mironov, A V Starobor, A G Vyatkin, and I A Ivanov for their assistance and helpful discussions, as well as to A M Sergeev and D Reitze for involving the author in the investigation of thermal effects in Faraday isolators and their constant encouragement and interest in the work. This study was supported by the Government of the Russian Federation under megagrant No. 14.B25.31.0024 based at the Institute of Applied Physics of the Russian Academy of Sciences and a grant from the governmental assignment No. 0035-2014-0016.

## References


1. Maiman T H *Nature* **187** 493 (1960)
2. Basov N G, Krokhin O N *Sov. Phys. JETP* **19** 123 (1964); *Zh. Eksp. Teor. Fiz.* **46** 171 (1964)
3. Gertsenshtein M E, Pustovoit V I *Sov. Phys. JETP* **16** 433 (1963); *Zh. Eksp. Teor. Fiz.* **43** 605 (1962)
4. Abbott B P et al. (LIGO Scientific Collab., Virgo Collab.) *Phys. Rev. Lett.* **116** 061102 (2016)
5. Quelle F W (Jr.) *Appl. Opt.* **5** 633 (1966)
6. Sims S D, Stein A, Roth C *Appl. Opt.* **6** 579 (1967)
7. Anan'ev Yu A et al. *J. Appl. Spectrosc.* **5** 36 (1966); *Zh. Prikl. Spektrosk.* **5** 51 (1966)
8. Mezenov A V, Soms L N, Stepanov A I *Termooptika Tverdotel'nykh Lazerov* (Thermooptics of Solid-State Lasers) (Leningrad: Mashinostroenie, 1986)
9. Anan'ev Yu A, Grishmanova N I *J. Appl. Spectrosc.* **12** 503 (1970); *Zh. Prikl. Spektrosk.* **12** 668 (1970)
10. Mak A A, Mit'kin V M, Soms L N *Optiko-Mekh. Promyshlennost'* **9** 65 (1971)
11. Vitrishchak I B, Soms L N, Tarasov A A *Sov. Phys. Tech. Phys.* **19** 664 (1974); *Zh. Tekh. Fiz.* **44** 1055 (1974)
12. Kertes I et al. *Sov. Phys. JETP* **32** 606 (1971); *Zh. Eksp. Teor. Fiz.* **59** 1115 (1970)
13. Foster J D, Osterink L M *J. Appl. Phys.* **41** 3656 (1970)
14. Massey G A *Appl. Phys. Lett.* **17** 213 (1970)
15. Koechner W *Appl. Opt.* **9** 1429 (1970)
16. Koechner W, Rice D K *IEEE J. Quantum Electron.* **6** 557 (1970)
17. Karr M A *Appl. Opt.* **10** 893 (1971)
18. Koechner W, Rice D K *J. Opt. Soc. Am.* **61** 758 (1971)
19. Soms L N, Tarasov A A, Shashkin V V *Sov. J. Quantum Electron.* **10** 350 (1980); *Kvantovaya Elektron.* **7** 619 (1980)
20. Soms L N, Tarasov A A *Sov. J. Quantum Electron.* **9** 1506 (1979); *Kvantovaya Elektron.* **6** 2546 (1979)
21. Scott W C, de Wit M *Appl. Phys. Lett.* **18** 3 (1971)
22. Giuliani G, Ristori P *Opt. Commun.* **35** 109 (1980)
23. Chen X, Gonzalez S *Appl. Phys. B* **67** 611 (1998)
24. Chen X, Chaux R *Opt. Commun.* **171** 119 (1999)
25. Dabby F W et al. *Appl. Phys. Lett.* **16** 362 (1970)
26. Chen X et al. *Opt. Commun.* **153** 301 (1998)
27. Klein C A *Opt. Eng.* **29** 343 (1990)
28. Klein C A *Opt. Eng.* **36** 1586 (1997)
29. Peng Y et al. *Appl. Opt.* **43** 6465 (2004)
30. Loze M K, Wright C D *Appl. Opt.* **37** 6822 (1998)
31. Shih O W *J. Appl. Phys.* **75** 4382 (1994)
32. Strain K A et al. *Phys. Lett. A* **194** 124 (1994)
33. Uehara N et al. *Proc. SPIE* **2989** 57 (1997)
34. Winkler W et al. *Opt. Commun.* **112** 245 (1994)
35. Khristov I P, Tomov I V, Saltiel S M *Opt. Quantum Electron.* **15** 289 (1983)
36. Eimerl D *IEEE J. Quantum Electron.* **23** 2238 (1987)
37. Hon D *IEEE J. Quantum Electron.* **12** 148 (1976)
38. Eimerl D *IEEE J. Quantum Electron.* **23** 575 (1987)
39. Horowitz M et al. *Opt. Lett.* **17** 475 (1992)
40. Andreev N, Khazanov E, Pasmanik G *IEEE J. Quantum Electron.* **28** 330 (1992)
41. Buzyalis R R, Dementev A S, Kosenko E K *Opt. Spectrosc.* **56** 458 (1984); *Opt. Spektrosk.* **56** 749 (1984)
42. Rayleigh Lord *Philos. Trans. R. Soc. Lond.* **176** 343 (1885)
43. Faraday M *Philos. Trans. R. Soc. Lond.* **136** 1 (1846)
44. Andreev N F, Palashov O V, Pasmanik G A, Khazanov E A *Quantum Electron.* **27** 565 (1997); *Kvantovaya Elektron.* **24** 581 (1997)
45. Andreev N et al. *IEEE J. Quantum Electron.* **35** 110 (1999)
46. Khazanov E A et al., in *Proc. Conf. on Lasers and Electro-Optics* (San Francisco, CA, 1998) p. 250
47. Khazanov E A *Quantum Electron.* **29** 59 (1999); *Kvantovaya Elektron.* **26** 59 (1999)
48. Khazanov E A et al. *IEEE J. Quantum Electron.* **35** 1116 (1999)
49. Khazanov E et al. *J. Opt. Soc. Am. B* **17** 99 (2000)
50. Andreev N F et al. *J. Opt. Technol.* **67** 556 (2000); *Opt. Zh.* **67** (6) 66 (2000)
51. Khazanov E A *Quantum Electron.* **30** 147 (2000); *Kvantovaya Elektron.* **30** 147 (2000)
52. Andreev N F et al. *Quantum Electron.* **30** 1107 (2000); *Kvantovaya Elektron.* **30** 1107 (2000)
53. Khazanov E A *Quantum Electron.* **31** 351 (2001); *Kvantovaya Elektron.* **31** 351 (2001)
54. Khazanov E et al. *Appl. Opt.* **41** 483 (2002)
55. Mueller G et al. *Class. Quantum Grav.* **19** 1793 (2002)
56. Khazanov E A et al. *Appl. Opt.* **41** 2947 (2002)
57. Andreev N F et al. *Quantum Electron.* **32** 91 (2002); *Kvantovaya Elektron.* **32** 91 (2002)
58. Jones R C *J. Opt. Soc. Am.* **31** 488 (1941)
59. Tabor W J, Chen F S *J. Appl. Phys.* **40** 2760 (1969)
60. Vyatkin A G, Snetkov I L, Palashov O V, Khazanov E A, in *Proc. CLEO/QELS 2013* (San Jose CA, 2013) paper CTu1O.5
61. Starobor A, Palashov O *Opt. Commun.* **354** 103 (2015)
62. Nicklaus K et al. *Adv. Solid-State Photon.* MB7 (2006)
63. Voitovich A V et al. *Quantum Electron.* **37** 471 (2007); *Kvantovaya Elektron.* **37** 471 (2007)
64. Mukhin I B, Voitovich A V, Palashov O V, Khazanov E A *Opt. Commun.* **282** 1969 (2009)
65. Snetkov I L, Mukhin I B, Palashov O V, Khazanov E A *Opt. Express* **19** 6366 (2011)
66. Snetkov I L, Palashov O V *Appl. Phys. B* **109** 239 (2012)
67. Mironov E A et al. *Quantum Electron.* **43** 740 (2013); *Kvantovaya Elektron.* **43** 740 (2013)
68. Snetkov I L, Voitovich A V, Palashov O V, Khazanov E A *IEEE J. Quantum Electron.* **50** 434 (2014)
69. Yasuhara R et al. *Opt. Lett.* **39** 1145 (2014)
70. Zheleznov D et al. *Opt. Express* **22** 2578 (2014)
71. Zheleznov D et al. *Opt. Lett.* **39** 2183 (2014)
72. Mironov E A, Palashov O V *Opt. Express* **22** 23226 (2014)
73. Nicklaus K, Langer T *Proc. of SPIE* **7578** 75781U (2010)
74. Snetkov I L et al., in *Proc. CLEO/Europe-IQEC* (2015)
75. Martinelli M *Opt. Commun.* **72** 341 (1989)
76. Bhandari R *Opt. Commun.* **88** 1 (1992)
77. Gelikonov V M et al. *Sov. Tech. Phys. Lett.* **13** 322 (1987); *Pis'ma Zh. Tekh. Fiz.* **13** 775 (1987)
78. Kawashima T et al. *Proc. SPIE* **3889** 596 (2000)
79. Nakai S et al. *Proc. SPIE* **4065** 29 (2000)
80. Carr I D, Hanna D C *Appl. Phys. B* **36** 83 (1985)
81. Sherman J *Appl. Opt.* **37** 7789 (1998)
82. Ostermeyer M R et al. *Appl. Opt.* **41** 7573 (2002)
83. Moshe I, Jackel S *Appl. Opt.* **39** 4313 (2000)
84. Jackel S M, Kaufman A *Opt. Eng.* **33** 3008 (1994)
85. Denman C A, Libby S I *Adv. Solid State Lasers* **26** 608 (1999)
86. Gelikonov V M, Leonov V I, Novikov M A *Quantum Electron.* **19** 1227 (1989); *Kvantovaya Elektron.* **16** 1905 (1989)
87. Yamashita S, Hotate K, Ito M *J. Lightwave Technol.* **14** 385 (1996)
88. Olsson N A *Electron. Lett.* **24** 1075 (1988)
89. Khazanov E *Appl. Opt.* **43** 1907 (2004)
90. Strehl K *Z. Instrumentenkunde* **22** 213 (1902)
91. Born M, Wolf E *Principles of Optics* (Cambridge: Cambridge Univ. Press, 1999)
92. Siegman A E *Proc. SPIE* **1224** 2 (1990)
93. Perevezentsev E, Poteomkin A, Khazanov E A *Appl. Opt.* **46** 774 (2007)
94. Vlasov S N, Petrishchev V A,Talanov V I *Radiophys. Quantum Electron.* 1062 (1971); *Izv. Vyssh. Uchebn. Zaved. Radiofiz.* **14** 1353 (1971)
95. Potemkin A K, Khazanov E A *Quantum Electron.* **35** 1042 (2005); *Kvantovaya Elektron.* **35** 1042 (2005)
96. Zheleznyakov V V, Kocharovskii V V, Kocharovskii V V *Sov. Phys. Usp.* **26** 877 (1983); *Usp. Fiz. Nauk* **141** 257 (1983)
97. Azzam R M A, Bashara N M *Ellipsometry and Polarized Light* (Amsterdam: North-Holland, 1977); Translated into Russian: *Ellipsometriya i Polyarizovannyi Svet* (Moscow: Mir, 1981)
98. Khazanov E "Faraday isolators for high average power lasers", in *Advances in Solid State Lasers Development and Applications* (Ed. M Grishin) (Rijeka: INTECH, 2010)
99. Khazanov E A *Opt. Lett.* **27** 716 (2002)
100. Snetkov I L, Mukhin I B, Palashov O V, Khazanov E A *Quantum Electron.* **37** 633 (2007); *Kvantovaya Elektron.* **37** 633 (2007)
101. Kagan M A, Khazanov E A *Quantum Electron.* **33** 876 (2003); *Kvantovaya Elektron.* **33** 876 (2003)
102. Kagan M A, Khazanov E A *Appl. Opt.* **43** 6030 (2004)
103. Vyatkin A G, Khazanov A E *J. Opt. Soc. Am. B* **29** 10 (2012)
104. Snetkov I L et al. *Opt. Express* **21** 21254 (2013)
105. Shiraishi K, Tajima F, Kawakami S *Opt. Lett.* **11** 82 (1986)
106. Mironov E A et al. *Opt. Lett.* **40** 2794 (2015)

107. Palashov O V et al. *J. Opt. Soc. Am. B* **29** 1784 (2012)
108. Yasuhara R et al. *Appl. Phys. Lett.* **105** 241104 (2014)
109. Snetkov I, Palashov O *Opt. Mater.* **42** 293 (2015)
110. Snetkov I L et al. *Opt. Express* **22** 4144 (2014)
111. Palashov O V et al. *Quantum Electron.* **41** 858 (2011); *Kvantovaya Elektron.* **41** 858 (2011)
112. Buhrer C F *Opt. Lett.* **14** 1180 (1989)
113. Mironov E A, Voitovich A V, Palashov O V *Laser Phys. Lett.* **13** 035001 (2016)
114. The VIRGO Collab. *Appl. Opt.* **47** 5853 (2008)
115. Katherin L D et al. *Rev. Sci. Instrum.* **83** 033109 (2012)
116. Mansell J D et al. *App. Opt.* **40** 366 (2001)
117. Khazanov E A et al. *IEEE J. Quantum Electron.* **40** 1500 (2004)
118. Zelenogorsky V, Palashov O, Khazanov E *Opt. Commun.* **278** 8 (2007)
119. Joiner R E, Marburger J, Steier W H *Appl. Phys. Lett.* **30** 485 (1977)
120. Snetkov I L, Vyatkin A G, Palashov O V, Khazanov E A *Opt. Express* **20** 13357 (2012)
121. Karimov D N et al. *Crystallogr. Rep.* **59** 718 (2014); *Kristallografiya* **59** 788 (2014)
122. Zelmon D E et al. *Appl. Opt.* **55** 834 (2016)
123. Padula C F, Young C G *IEEE J. Quantum Electron.* **3** 493 (1967)
124. Zheleznov D S et al. *Quantum Electron.* **36** 383 (2006); *Kvantovaya Elektron.* **36** 383 (2006)
125. Barnes N P, Petway L P *J. Opt. Soc. Am. B* **9** 1912 (1992)
126. Valiev U V et al. *Sov. Phys. Solid State* **24** 1596 (1982); *Fiz. Tverd. Tela* **24** 2818 (1982)
127. Yasuhara R et al. *Opt. Express* **15** 11255 (2007)
128. Zheleznov D S, Starobor A V, Palashov O V, Khazanov E A *J. Opt. Soc. Am. B* **29** 786 (2012)
129. Starobor A V, Zheleznov D S, Palashov O V, Khazanov E A *J. Opt. Soc. Am. B* **28** 1409 (2011)
130. Slack G A, Oliver D W *Phys. Rev. B* **4** 592 (1971)
131. Rothhardt C et al. *Proc. SPIE* **8601** 86010T (2013)
132. Mironov E A et al. *Appl. Opt.* **53** 3486 (2014)
133. Mironov E A et al. *Appl. Opt.* **51** 5073 (2012)
134. Mironov E A, Voitovich A V, Palashov O V *Opt. Commun.* **295** 170 (2013)
135. Zheleznov D S et al. *Quantum Electron.* **40** 276 (2010); *Kvantovaya Elektron.* **40** 276 (2010)
136. Zheleznov D S et al. *IEEE J. Quantum Electron.* **43** 451 (2007)
137. Starobor A V, Zheleznov D S, Palashov O V *IEEE J. Quantum Electron.* **48** 1120 (2012)
138. Robinson C C *Appl. Opt.* **3** 1163 (1964)
139. Weber M J *Proc. SPIE* **681** 75 (1986)
140. Johnston T F, Proffitt W *IEEE J. Quantum Electron.* **16** 483 (1980)
141. Mukhin I B, Palashov O V, Khazanov E A, Ivanov I A *JETP Lett.* **81** 90 (2005); *Pis'ma Zh. Eksp. Teor. Fiz.* **81** 120 (2005)
142. Vyatkin A G, Khazanov E A *J. Opt. Soc. Am. B* **28** 6 (2011)
143. Geho M, Sekijima T, Fujii T *J. Cryst. Growth* **267** 188 (2004)
144. Lin H, Zhou S, Teng H *Opt. Mater.* **33** 1833 (2011)
145. Ganschow S et al. *Proc. SPIE* **3178** 55 (1997)
146. Valiev U V et al. *J. Luminesc.* **176** 86 (2016)
147. Pawlak D A et al. *J. Cryst. Growth* **226** 341 (2001)
148. Shimamura K, Villora E G *Acta Phys. Polon. A* **124** 265 (2013)
149. Villora E G et al. *Appl. Phys. Lett.* **99** 011111 (2011)
150. Shimamura K et al. *Crystal Growth Design* **10** 3466 (2010)
151. Furuse H et al. *Opt. Mater. Express* **6** 191 (2015)
152. Starobor A, Palashov O, Zhou S *Opt. Lett.* **41** 1510 (2016)
153. Chen Z et al. *Mater. Lett.* **145** 171 (2015)
154. Chen Z et al. *Mater. Lett.* **161** 93 (2015)
155. Wang X et al. *J. Alloys Comp.* **649** 1085 (2015)
156. Chen Z et al. *Opt. Lett.* **40** 820 (2015)
157. Guo F et al. *Opt. Mater.* **47** 543 (2015)
158. Guo F Y et al. *J. Cryst. Growth* **397** 19 (2014)
159. Kang J et al. *Opt. Mater.* **36** 1266 (2014)
160. Mei M et al. *Adv. Mater. Res.* **306–307** 1722 (2011)
161. Chen X et al. *Opt. Mater.* **37** 188 (2014)
162. Guo F et al. *Opt. Mater.* **35** 227 (2012)
163. Chen X et al. *J. Cryst. Growth* **421** 8 (2015)
164. Liu J et al. *J. Cryst. Growth* **310** 2613 (2008)
165. Veber P et al. *CrystEngComm* **17** 492 (2015)
166. Snetkov I L et al. *Appl. Phys. Lett.* **108** 161905 (2016)
167. Snetkov I L et al. *IEEE J. Quantum Electron.* **51** (2015)
168. Mironov E A et al. *Opt. Lett.* **40** 4919 (2015)
169. Zheleznov D S, Starobor A V, Palashov O V *Opt. Mater.* **46** 526 (2015)
170. Kruk A et al. *Opt. Appl.* **45** 585 (2015)
171. Vyatkin A G *IEEE J. Quantum Electron.* **50** 1061 (2014)
172. Vyatkin A G, Khazanov E A *IEEE J. Quantum Electron.* **51** 1700108 (2015)
173. Valiev U V et al. *J. Appl. Phys.* **104** 073903 (2008)
174. Zelenogorskii V V, Khazanov E A *Quantum Electron.* **40** 40 (2010); *Kvantovaya Elektron.* **40** 40 (2010)
175. Avakyants L I et al. *Quantum Electron.* **8** 423 (1978); *Kvantovaya Elektron.* **5** 724 (1978)
176. Demskaya E L, Prokhorova T I *Fiz. Khim. Stekla* **9** 554 (1983)
177. Savinkov V I et al. *J. Non-Cryst. Solids* **356** 1655 (2010)
178. Starobor A V et al. *Opt. Commun.* **358** 176 (2016)
179. Jackson W B et al. *Appl. Opt.* **20** 1333 (1981)
180. Alexandrovski A et al. *Proc. of SPIE* **7193** 71930D (2009)
181. Kuznetsov I et al. *Opt. Mater. Express* **4** 2204 (2014)
182. Sato Y, Taira T *Opt. Express* **14** 10528 (2006)
183. Morikawa J, Hashimoto T *Jpn. J. Appl. Phys.* **37** L1484 (1998)
184. Gauthier D J, Narum P, Boyd R W *Opt. Lett.* **11** 623 (1986)
185. Geho M et al. *Jpn. J. Appl. Phys.* **44** 4967 (2005)
186. Birch K P *Opt. Commun.* **43** 79 (1982)
187. Trénec G et al. *Appl. Opt.* **50** 4788 (2011)
188. Mironov E A et al. *Quantum Electron.* **43** 740 (2013); *Kvantovaya Elektron.* **43** 740 (2013)
189. Mironov E A, Voitovich A V, Palashov O V *Quantum Electron.* **41** 71 (2011); *Kvantovaya Elektron.* **41** 71 (2011)
190. Nicklaus K, Seyffert G, US Patent US20120194906 A1 (2009)
191. Mukhin I B, Khazanov E A *Quantum Electron.* **34** 973 (2004); *Kvantovaya Elektron.* **34** 973 (2004)
192. Zheleznov D S, Khazanov E À, Mukhin I B, Palashov V *Proc. SPIE* **6610** 66100F (2007)
193. Mironov E A et al. *Opt. Commun.* **338** 565 (2015)
194. Zarubina T V, Petrovsky G T *J. Opt. Technol.* **59** 700 (1992); *Opt. Zh.* **59** (11) 48 (1992)
195. Zarubina T V et al. *J. Opt. Technol.* **64** 1041 (1997); *Opt. Zh.* **64** (11) 67 (1997)
196. Chen X et al. *Solid-State Electron.* **42** 1765 (1998)
197. Jiang Y, Myers M J, Rhonenhouse D *Proc. SPIE* **1761** 268 (1992)
198. Kaminskii A A et al. *Laser Phys. Lett.* **2** 489 (2005)
199. Raja M Y A, Allen D, Sisk W *Appl. Phys. Lett.* **67** 2123 (1995)
200. Ivanov I et al., in *Proc. CLEO/EUROPE-EQEC 2009* (Munich, Germany, 2009) p. CE.P.12
201. Chen X et al. *Solid State Commun.* **110** 431 (1999)
202. Yasuhara R, Furuse H *Opt. Lett.* **38** 1751 (2013)
203. Yasuhara R et al. *Opt. Express* **21** 31443 (2013)
204. Starobor A et al. *Opt. Mater.* **47** 112 (2015)
205. Starobor A V, Zheleznov D S, Palashov O V *Laser Phys.* **26** 025801 (2016)
206. Malshakov A N, Pasmanik G, Poteomkin A K *Appl. Opt.* **36** 6403 (1997)
207. Zarubina T V, Private communication (2000)
208. Davis J A, Bunch R M *Appl. Opt.* **23** 633 (1984)